7. Dawson WW, Radtke ND (1977) The electrical stimulation of the retina by indwelling electrodes. Invest Ophthalmol Vis Sci 16:249–252
8. Dobelle WH (2000) Artificial vision for the blind by connecting a television camera to the visual cortex. ASAIO J 46:3–9
9. Dobelle WH, Mladejovsky MG, Evans JR, Roberts TS, Girvin JP (1976) "Braille" reading by a blind volunteer by visual cortex stimulation. Nature 259:111–112
10. Dobelle WH, Mladejovsky MG, Girvin JP (1974) Artificial vision for the blind: electrical stimulation of visual cortex offers hope for a functional prosthesis. Science 183:440–444
11. Dobelle WH, Turkel J, Henderson DC, Evans JR (1979) Mapping the representation of the visual field by electrical stimulation of human visual cortex. Am J Ophthalmol 88:727–735
12. Drasdo N, Aldebasi YH, Chiti Z, Mortlock KE, Morgan JE, North RV (2001) The SCone PhNR and Pattern ERG in Primary Open Angle Glaucoma. Invest Ophthalmol Vis Sci 42:1266–1272
13. Eckhorn R, Stett A, Schanze T, Gekeler F, Schwahn H, Zrenner E, Wilms M, Eger M, Hesse L (2001) Physiological functional evaluation of retinal implants in animal models. Ophthalmologe 98:369–375 [in German]
14. Gekeler F, Schwahn HN, Stett A, Kohler K, Zrenner E (2001) Subretinal microphotodiodes to replace photoreceptor-function: a review of the current state. In: Doly M, Droy M-T, Christen Y (eds) Vision, sensations et environment, Irvinn, Paris, pp 77–95
15. Hesse L, Schanze T, Wilms M, Eger M (2000) Implantation of retina stimulation electrodes and recording of electrical stimulation responses in the visual cortex of the cat. Graefes Arch Clin Exp Ophthalmol 238:840–845
16. Humayun MS, de Juan EJ (1998) Artificial vision. Eye 12:605–607
17. Humayun MS, de Juan EJ, Dagnelie G, Greenberg RJ, Propst RH, Phillips DH (1996) Visual perception elicited by electrical stimulation of retina in blind humans. Arch Ophthalmol 114:40–46
18. Humayun MS, de Juan EJ, Weiland JD, Dagnelie G, Katona S, Greenberg R, Suzuki S (1999) Pattern electrical stimulation of the human retina. Vision Res 39:2569–2576
19. Humayun MS, Prince M, de Juan EJ, Barron Y, Moskowitz M, Klock IB, Milam AH (1999) Morphometric analysis of the extramacular retina from postmortem eyes with retinitis pigmentosa. Invest Ophthalmol Vis Sci 40:143–148
20. Humayun MS, Propst RH, de Juan EJ, McCormick K, Hickingbotham D (1994) Bipolar surface electrical stimulation of the vertebrate retina. Arch Ophthalmol 112:110–116
21. Humayun MS, Weiland JD, de Juan EJ (1999) Electrical stimulation of the human retina. In: Hollyfield JG, Anderson RE, LaVail MM (eds) Retinal degenerative diseases and experimental therapy. Kluwer Academic /Plenum Publishers, New York, p 479
22. Kohler K, Hartmann JA, Werts D, Zrenner E (2001) Histological studies of retinal degeneration and biocompatibility of subretinal implants. Ophthalmologe 98:364–368
23. Milam AH, Li ZY, Fariss RN (1998) Histopathology of the human retina in retinitis pigmentosa. Prog Retin Eye Res 17:175–205
24. Normann RA, Maynard EM, Guillory KS, Warren DJ (1996) Cortical implants for the blind. IEEE Spectrum 33:54–59
25. Normann RA, Maynard EM, Rousche PJ, Warren DJ (1999) A neural interface for a cortical vision prosthesis. Vision Res 39:2577–2587
26. Pardue MT, Stubbs EB Jr, Perlman JI, Narfstrom K, Chow AY, Peachey NS (2001) Immunohistochemical studies of the retina following long-term implantation with subretinal microphotodiode arrays. Exp Eye Res 73:333–343
27. Peyman G, Chow AY, Liang C, Chow VY, Perlman JI, Peachey NS (1998) Subretinal semiconductor microphotodiode array. Ophthalmic Surg Lasers 29:234–241
28. Rizzo JF, Loewenstein J, Wyatt JL (1999) Development of an epiretinal electronic visual prosthesis: the Harvard Medical School–Massachusetts Institute of Technology Research Program. In: Hollyfield JG, Anderson RE, LaVail MM (eds) Retinal degenerative diseases and experimental therapy. Kluwer Academic /Plenum Publishers, New York, p 463
29. Ronner SF, Foote WE, Feldon SE (1980) Activation of single cells in cat visual cortex by electrical stimulation of the cortical surface. Exp Neurol 70:47–64
30. Santos A, Humayun MS, de Juan EJ, Greenburg RJ, Marsh MJ, Klock IB, Milam AH (1997) Preservation of the inner retina in retinitis pigmentosa. A morphometric analysis. Arch Ophthalmol 115:511–515
31. Schmidt EM, Bak M, Hambrecht FT, Kufta CV, O'Rourke DK, Vallabhanath P (1996) Feasibility of a visual prosthesis for the blind based on intracortical microstimulation of the visual cortex. Brain 119:507–522
32. Schwahn HN, Gekeler F, Kohler K, Kobuch K, Sachs HG, Schulmeyer F, Jakob W, Gabel VP, Zrenner E (2001) Studies on the feasibility of a subretinal visual prosthesis: data from Yucatan micropig and rabbit. Graefes Arch Clin Exp Ophthalmol 239:961–967
33. Schwahn HN, Gekeler F, Kohler K, Zrenner E (2001) Stimulation des visuellen Systems durch subretinale Elektrostimulation: Tierexperimentelle Daten zur Machbarkeit einer subretinalen Netzhautprothese. Nova Acta Leopoldina NF 84:209–221
34. Stett A, Barth W, Weiss S, Haemmerle H, Zrenner E (2000) Electrical multisite stimulation of the isolated chicken retina. Vision Res 40:1785–1795
35. Stieglitz T, Blau C, Beutel H, Keller R, Meyer JU (1997) Conception and development of flexible stimulator structures within a retinal implant system] Konzeption und Entwicklung von flexiblen Stimulatorstrukturen innerhalb eines Retina Implantat Systems. Biomed Tech Berl 42 (Suppl):458–459 [in German]
36. Veraart C, Raftopoulos C, Mortimer JT, Delbeke J, Pins D, Michaux G, Vanlierde A, Parrini S, Wanet-Defalque MC (1998) Visual sensations produced by optic nerve stimulation using an implanted self-sizing spiral cuff electrode. Brain Res 813:181–186
37. Volker M, Gekeler F, Shinoda K, Sachs H, Gmeiner H, Kohler K, Inhoffen W, Bartz-Schmidt KU, Zrenner E (2002) Implantation of Microphotodiode Arrays (MPDA) in cats: OCT and fluorescein angiography. Invest Ophthalmol Vis Sci (abstract)
38. Walter P, Heimann K (2000) Evoked cortical potentials after electrical stimulation of the inner retina in rabbits. Graefes Arch Clin Exp Ophthalmol 238:315–318
39. Walter P, Szurman P, Vobig M, Berk H, Ludtke-Handjery HC, Richter H, Mittermayer C, Heimann K, Sellhaus B (1999) Successful long-term implantation of electrically inactive epiretinal microelectrode arrays in rabbits. Retina 19:546–552
40. Yagi T, Ito Y, Kanda H, Tanaka S, Watanabe M, Uchikawa Y (1994) Hybrid retinal implant: fusion of engineering and neuroscience. IEEE 4:382–385
41. Yamamoto S, Yamamoto T, Hayashi M, Takeuchi S (2001) Morphological and functional analyses of diabetic macular edema by optical coherence tomography and multifocal electroretinograms. Graefes Arch Clin Exp Ophthalmol 239:96–101

42. Zrenner E The spectral properties of the human visual Ssystem as revealed by visually evoked cortical potentials/ VECP) and psychophysical investigations. In: Braitenberg V, Barlow HB, Bullock H, Florey E, Grüsser OJ, Peters A (eds) Neurophysiological aspects of color vision in primates. Springer, Berlin Heidelberg New York, pp 112–172
43. Zrenner E (2002) Will retinal implants restore vision? Science 295:1022–1025
44. Zrenner E, Gekeler F, Gabel VP, Graf HG, Graf M, Guenther E, Haemmerle H, Hoefflinger B, Kobuch K, Kohler K, Nisch W, Sachs H, Schlosshauer B, Schubert M, Schwahn H, Stelzle M, Stett A, Troeger B, Weiss S (2001) Subretinal microphotodiode array as replacement for degenerated photoreceptors?. Ophthalmologe 98:357–363
45. Zrenner E, Miliczek K-D, Gabel V-P, Graf HG, Guenther E, Haemmerle H, Hoefflinger B, Kohler K, Nisch W, Schubert M, Stett A, Weiss S (1997) The development of subretinal microphotodiodes for replacement of degenerated photoreceptors [see comments]. Ophthalmic Res 29:269–280
46. Zrenner E, Stett A, Weiss S, Aramant RB, Guenther E, Kohler K, Miliczek K-D, Seiler MJ, Haemmerle H (1999) Can subretinal microphotodiodes successfully replace degenerated photoreceptors? Vision Res 39:2555–2567
47. Zrenner E, Weiss S, Stett A, Brunner B, Gabel V-P, Graf M, Graf HG, Haemmerle H, Hoefflinger B, Kobuch K, Miliczek K-D, Nisch W, Sachs H, Stelzle M (1999) Are subretinal microphotodiodes suitable as a replacement for degenerated photoreceptor? In: Hollyfield JG, Anderson RE, LaVail MM (eds) Retinal degenerative diseases and experimental therapy. Kluwer Academic /Plenum Publishers, New York, pp 497–506

Available online at www.sciencedirect.com
SCIENCE DIRECT®
Vision Research 44 (2004) 1033–1038
Vision Research
www.elsevier.com/locate/visres

New method for detecting misrouted retinofugal fibers in humans with albinism by magnetoencephalography ☆

Hisao Ohde [a,*], Kei Shinoda [a], Takatsune Nishiyama [a], Hisashi Kado [b], Yasuhiro Haruta [b], Yukihiko Mashima [a], Yoshihisa Oguchi [a]

[a] Department of Ophthalmology, Keio University School of Medicine, 35 Shinanomachi, Shinjuku, Tokyo 160-8582, Japan
[b] Applied Electronics Laboratory, Kanazawa Institute of Technology, Amaikecho, Kanazawa-shi, Ishikawa 920-1331, Japan

Received 30 July 2003; received in revised form 9 December 2003

Abstract

In humans with albinism, a large percentage of the ganglion cell axons from the temporal retina decussate abnormally in the chiasm and synapse in the contralateral LGN. The aim of this study was to determine whether the misrouting of the optic fibers can be detected by magnetoencephalography (MEG). Visually evoked magnetic fields (VEFs) were recorded from three patients with albinism. After monocular stimulation, the isofield contour maps of the VEFs showed a single current dipole pattern over the contralateral hemisphere in patients with albinism. These results clearly illustrated the reduced uncrossed retinofugal pathway of patients with albinism.

Keywords: Albinism; Central visual pathway; Electrophysiology; Visual evoked magnetic field; Magnetoencephalography

1. Introduction

Albinism is a heterogeneous group of inherited (usually autosomal recessive) disorders with deficiency or absence of pigment in the skin, hair, and eyes, or eyes only, due to an abnormality in the production of melanin. Lund (1965) was the first to report an abnormal decussation, namely a significantly smaller percentage of uncrossed retinotectal fibers, in albino rats. Since then, several other albinotic mammalian species have been shown to have a similar misrouting of retinofugal fibers resulting in a higher percentage of decussated fibers (Creel, 1971; Gross & Hickey, 1980; Guillery & Kaas, 1973; Sanderson, 1975).

Guillery, Okoro, and Witkop (1975) detected a morphological anomaly of the lateral geniculate nucleus in the brain of a human with albinism, and Creel, Witkop, and King (1974) demonstrated that the visually evoked cortical potentials (VEPs) elicited by monocular stimulation were significantly asymmetrical in the two hemispheres of subjects with albinism. The asymmetry was not present in most normally pigmented humans. These results were interpreted as indicating a reduction in the percentage of uncrossed retino-geniculo-cortical projection in patients with albinism.

There is conflicting evidence on whether an asymmetry is present in all patients with albinism because different stimulus conditions, e.g., pattern onset (Apkarian, 1992; Bouzas, Caruso, Drews-Bankiewicz, & Kaiser-Kupfer, 1994), pattern reversal (Carroll, Jay, McDonald, & Halliday, 1980), flash (Fizgerald & Cibis, 1994; Russell-Eggitt, Kriss, & Taylor, 1990), different recording conditions, and different response criteria were used (Fizgerald & Cibis, 1994). In addition, the sensitivity of detecting asymmetrical responses with the VEP ranged from 45% to 100% (Apkarian, Reits, Spekreijse, & Van Dorp, 1983; Bouzas et al., 1994; Soong, Levin, & Westall, 2000). These observations combined with the usual variability of VEPs, made it difficult to use VEPs in the clinic routinely to determine whether a misrouting of retinofugal fibers is present.

Magnetoencephalography (MEG) is a relatively new technique that can detect human neuronal activity of the brain (Barth, Sutherling, Engel, & Beatty, 1982; Cohen, 1972). The activity can be detected in real-time and a

☆ Grant-in-aid for Scientific Research (B)(2) 1999–2000.
* Corresponding author. Tel.: +81-3-3353-1211x62402; fax: +81-3-3359-8302.
E-mail address: hiohde@sc.itc.keio.ac.jp (H. Ohde).

0042-6989/$ - see front matter © 2004 Elsevier Ltd. All rights reserved.
doi:10.1016/j.visres.2003.12.005

good estimation of the source of the activity can be made. MEGs are not altered by the electric resistance of the tissue, e.g., bone, CSF, and meninges, which is a great advantage over the EEG. Recordings of the visually evoked magnetic fields (VEFs) with monocular light stimuli have shown bilateral dipole patterns in the occipital lobes of normal subjects (Oguchi, 1998).

Because MEGs can detect neuronal activity, we hypothesized that the VEFs recorded during monocular photic stimuli will be symmetrical in control pigmented subjects and asymmetrical in patients with albinism. To test this hypothesis, we recorded the VEFs during monocular and binocular light stimulation and compared the responses from controls to those from patients with albinism.

2. Subjects and methods

2.1. Subjects

Three patients with three different types of albinism, two with oculocutaneous and one with ocular albinism, were tested. These patients were the first three who were examined in our clinic after this MEG became available. The findings in these three patients with albinism were compared to those from three subjects with normal pigmentation and no eye diseases (control group), who were randomly selected volunteers in our department.

Case 1 was a 19-year-old woman who was a tyrosinase-negative oculocutaneous albino with complete absence of skin and hair pigmentation. She suffered from severe photophobia with complete transillumination of the irides. Visual acuity was 6/80 in both eyes with high myopia (OD, −16.0 diopters (D); OS, −18.0 D). Esotropia and nystagmus were present.

Case 2 was a 12-year-old young boy with tyrosinase-positive oculocutaneous albinism. He lacked skin pigmentation, his hair color was red, and his irides were light brown. He was not photophobic. Visual acuity was 6/20 in both eyes with high astigmatism. Exotropia and nystagmus were present.

Case 3 was a 16-year-old young boy with ocular albinism. His skin and hair were normally pigmented. His iridies were brown and he did not complain of photophobia. Visual acuity was 6/20 in both eyes with high astigmatism. Exotropia and nystagmus were present.

In all three patients, fundus examination revealed hypopigmentation with macular hypoplasia. Their visual fields were full.

The procedures used in this research followed the tenets of the Declaration of Helsinki, and informed consent was obtained from each subject after the nature of the study was explained. Where applicable, the research was approved by the KEIO University, School of Medicine Institutional Human Experimentation Committee.

2.2. Magnetoencephalographic (MEG) system

The MEG system was the whole-head type with a 160-channel superconducting quantum interference device (SQUID) based on a coaxial type gradiometer (Yokogawa Elec. Co., Japan). MEG recordings were made in a magnetically shielded room.

2.3. Photic stimulation

White, stroboscopic stimuli (ERG Photic Stimulator:Nihon Kohden) were presented monocularly or binocularly at 1 Hz with an intensity of 0.3 J. This stimulus intensity was equivalent to 2.5 candelas seconds per meter squared (cd s/m^2).

2.4. Recordings

VEFs were recorded with the whole-head 160-channel SQUID system during monocular or binocular photic stimulation. The analysis time was 500 ms, and each recording was the average of 200 responses. The sampling rate was 1.0 kHz, and the bandpass filter was set at 3 Hz–1 kHz with a 50 Hz notch filter. Two trials were performed at each session.

Magnetic resonance imaging (MRI) was performed with a GE Signa 1.5 Tesla system (GE Yokogawa Medical Systems, Japan). T1-weighted images with a contiguous 1.5 mm thick contiguous slices were used for overlays, with the equivalent current dipole (ECD) sources determined by MEG.

For MEGs and MRIs, five marker coils were placed on the skull for the subsequent analysis of the source of the VEFs by MRIs. Two of them were placed at the right and left pre-auricular points of the subject. The center marker was placed 5 cm above the nasion, and the other two frontal markers were placed 5 cm lateral to the center marker. Each marker coil generated a fixed ECD for which the intensity and direction were already known. The locations of each marker coil could be estimated precisely on the coordinate axes on the MEG alignment. To determine the origin of the coordinate axes on the MRI, the locations of the MRI markers and the locations of the marker coils, estimated with MEG, were aligned.

2.5. Analysis

Source analyses were based on a single- or two-ECD model for spherical volume conduction. The local responses from the 160 channels were recorded and superimposed to determine the implicit times of the three positive peaks at around 70, 100, and 150 ms

(arrows, Fig. 1, upper traces). The isofield contour maps of VEFs (M70, M100, and M150) at each implicit time with contour steps of 20 fT (femto Tesla; 10^{-15} T) were plotted according to the 160 local responses.

The isofield contour map at a specific implicit time was made in the following way. In the contour maps of Fig. 1, the blue dots show the location of each of the 160 SQUID sensors. The distribution of the magnetic field potential is represented in a contour map according to the amplitude at each recording point at the selected implicit time. The green lines represent the outward-going flux, and red lines represented the inward-going flux. The black line showed the zero point (middle of Fig. 1).

By using a single- or two-dipole theory, the ECDs were estimated and localized on the MRI (lower of Fig. 1). Goodness-of-fit values greater than 90% were considered to indicate a good dipole model.

3. Results

The VEFs consisted of three peaks which appeared at about 70 ms (M70), 100 ms (M100), and 150 ms (M150;

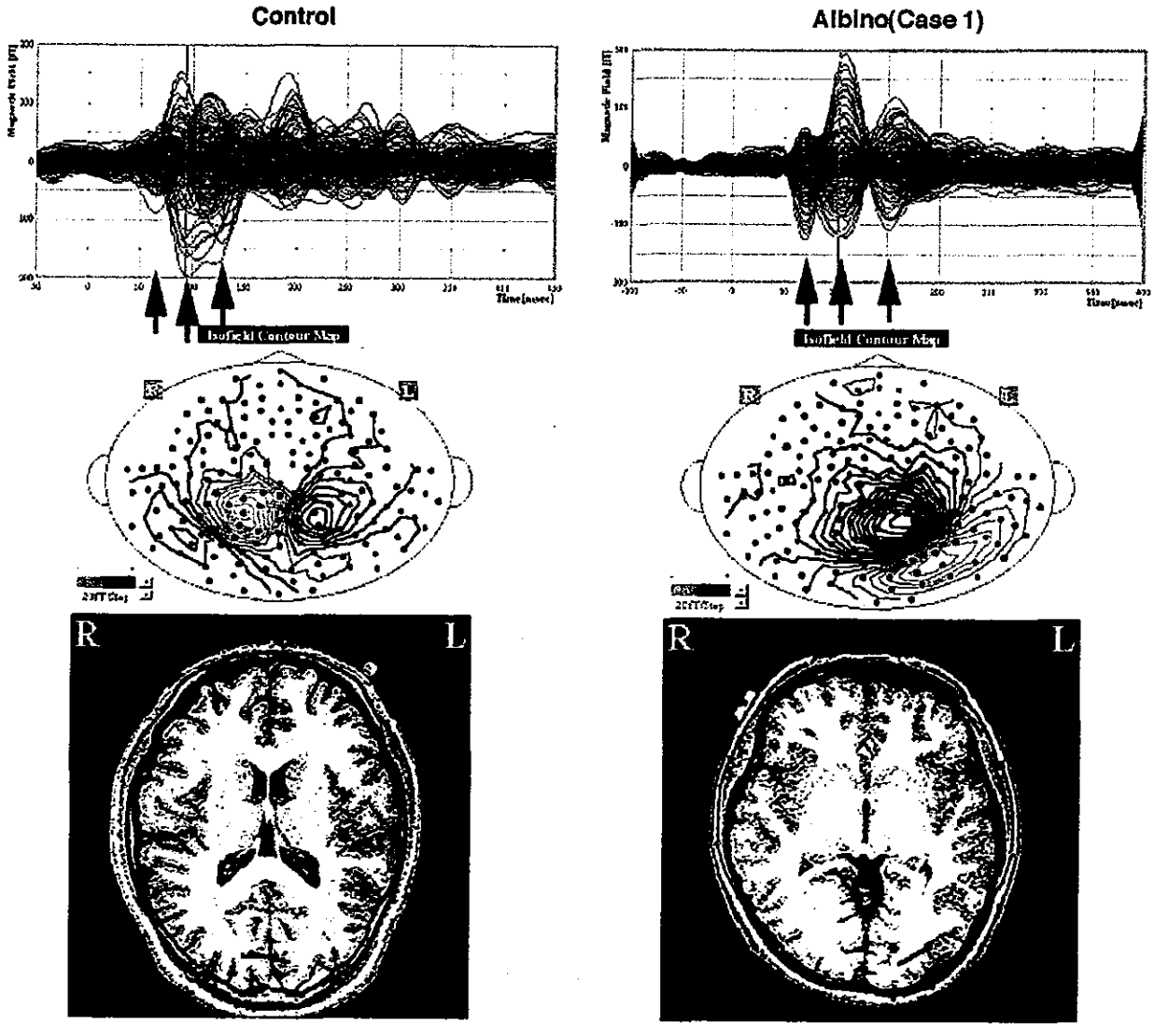

Fig. 1. Comparison of the visual evoked magnetic fields (VEFs) and the estimated current dipoles (ECDs) in a control subject and patient with albinism. The 160 VEFs were superimposed for the 160 local responses from each channel (upper). Three arrows point to the three peaks at about 70 ms (M70), 100 ms (M100), and 150 ms (M150). The isofield contour maps (middle) and estimated equivalent current dipoles (lower) with photic stimuli of the right eye are also shown. The middle row shows the results of the isofield contour maps at M100's implicit time in a control subject (left) and a patient with albinism (right), blue dots showed the location of each 160 SQUID sensors and outward-going flux is represented by green lines in the contour plot, inward-going flux by red lines, and the zero point by black line. The estimated ECDs are represented by red dots and lines; the red dot is the starting point of the ECDs and line shows the direction of the dipole (lower). In the control subject, both hemispheres of the primary visual cortex are activated (left), whereas mainly the contralateral hemisphere is activated in the albino patient (right).

Fig. 1). M100 is considered to be equivalent to the P100 component of VEPs and is the main response of the primary visual cortex (V1) (Hatanaka et al., 1997; Seki et al., 1996). The isofield contour maps and the estimated ECDs for the VEFs elicited by photic stimulation of the right eye are shown in Fig. 1 for one control subject and one patient with albinism. The MRI for each subject is shown in the lower set of Fig. 1.

3.1. Control subjects

The isofield contour map of the VEFs at M100 showed two ECDs that were estimated to be from both hemispheres of the occipital region after monocular stimulation of either eye (Fig. 1). The directions of these dipoles tended to cross the midline of the brain. A magnetic field pattern similar to that obtained by monocular stimulation was observed after binocular stimulation. As expected, the estimated ECDs obtained with binocular stimulation also demonstrated two opposite dipoles crossing the midline of the brain.

3.2. Patients with albinism

The isofield contour maps at M100 obtained from the response during monocular and binocular light stimulation for the three patients with albinism are shown in Fig. 2. In all three patients with albinism, the isofield contour maps at M100 showed a single current dipole over the occipital region contralateral to the stimulated eye during monocular stimulation (Fig. 2). In Cases 1 and 2, the implicit time of M100 was around 100 ms, and that of M150 was around 150 ms. The ECD of M100 was estimated to be on V1 of the hemisphere contralateral to the stimulated eye and was directed to the midline of the brain (Fig. 2). The isofield contour map of M150 also showed a single dipole pattern and the direction was opposite to that of M100.

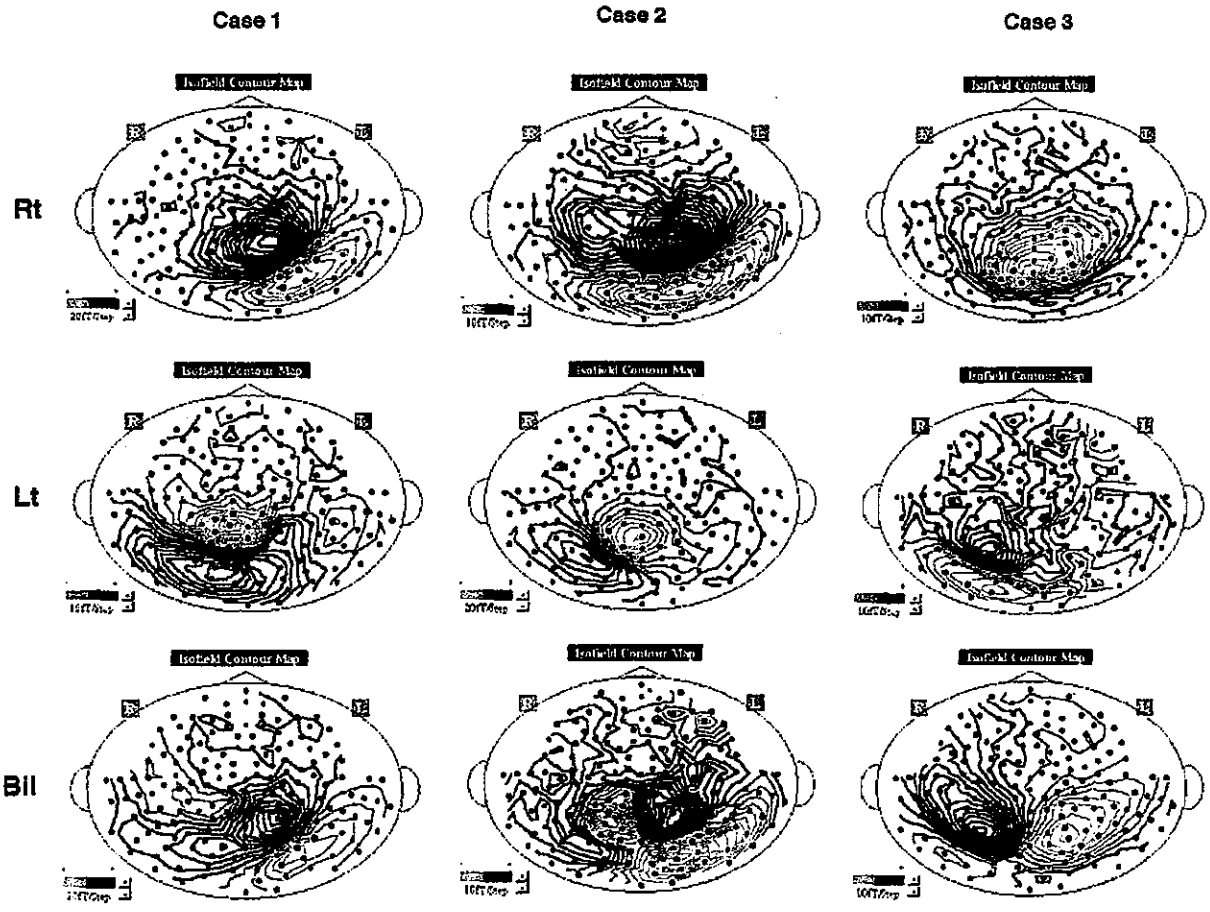

Fig. 2. The isofield contour maps at M100's implicit time of the three patients with albinism after monocular and binocular stimulation. In all three patients with albinism, light stimulation of the right eye activates the left hemisphere (upper), and stimulation for the left eye activates the right hemisphere (middle), and binocular stimulation activates both the right and left hemispheres of the posterior lobe (lower). According to the patterns of the contour maps, the directions of the dipoles in the oculocutaneous albinisms (Cases 1 and 2) should be toward the midline of the brain, which is opposite to the dipole in ocular albinism (Case 3).

In Case 3, the magnetic field pattern during monocular stimulation was slightly different from that in the other two cases. The implicit time of M100 was somewhat delayed to 110–120 ms and that of M150 was also delayed to 160–170 ms. The isofield contour maps of M100 and M150 demonstrated that the direction of the dipole was opposite to those of the other two cases suggesting an unusual anatomy of the calcarine sulcus (Fig. 2).

The implicit time of M100 and M150 in the VEFs elicited by binocular stimulation in Case 3 was delayed to 110–120 ms and to 160–170 ms, respectively. Two current isofield dipoles pattern comprising of M100 and M150 were estimated over the bilateral hemispheres of V1 after binocular stimulation in all three patients (Fig. 2).

4. Discussion

Our results clearly showed that in patients with albinism monocular light stimulation elicited only contralateral estimated ECDs, but in control subjects, ECDs were detected in both hemispheres and crossed the midline. Thus, we have demonstrated asymmetrical VEFs in patients with albinism just as the asymmetrical VEPs. As in the VEPs, the asymmetrical VEFs reflected the poor ipsialteral retinofugal projection.

In subjects with normal pigmentation and no eye disease, approximately 45% of ganglion cell axons from one eye remain uncrossed as they pass through the optic chiasm and project to the ipsilateral lateral geniculate nucleus (LGN). These uncrossed axons originate in the temporal half of the retina with the greatest population serving the central 20 deg. In contrast, the ganglion cell axons from the central temporal retina in patients with albinism decussate abnormally at the chiasm and project to the contralateral LGN, and most of the axons from the peripheral temporal retina remain ipsilateral. Thus, in humans with albinism, only 10–20% of axons from each retina remain uncrossed as opposed to 45% in subjects with normal pigmentation and no eye disease (McHam & Fulton, 1992).

According to Creel (1978), about 70% of human oculocutaneous albinos show asymmetrical VEPs, and at present, an asymmetrical VEP is the most reliable sign for an abnormal visual pathway in human with albinism. No explanation has been presented on why the other 30% of the patients with albinism do not show the asymmetrical responses.

Although only three cases were studied, the MEGs clearly showed an abnormal decussation in all cases. More data must be collected to establish this method as an established diagnostic tool for detecting abnormal decussation of visual pathway in human with albinism as well as to confirm the VEP findings.

Several other techniques have recently been reported to demonstrate the misrouting of the retinofugal fibers. Positron emission tomography (PET) showed asymmetric glucose metabolism in the posterior medial occipital cortex in patients with albinism (Nakagawa, Kiyosawa, Tamai, & Ito, 1993), and functional magnetic resonance imaging (f-MRI) also gave similar results (Hedera et al., 1994; Morland, Hoffmann, Neveu, & Holder, 2002). However, these tests do not measure neuronal activities directly, and their reliability in subjects with albinism has not been examined.

MEG is a relatively new technique that can detect very weak magnetic fields originating from neuronal electrical activities, and it can localize the source of the signals to functional regions of the brain by combining them with MR images. In addition, the VEFs recorded during visual stimulation can detect the neuronal activities in the primary visual cortices of both hemispheres thereby allowing real-time analysis of activation and localization of the visual signals. For example, the VEFs elicited by light stimuli were able to detect the hemianopsia in brain-damaged patients (Nakasato et al., 1996).

Our results showed that monocular photic stimulation activated only the contralateral hemisphere of the primary visual cortex in three patients with different types of albinism whereas monocular stimulation activated both hemispheres of the primary visual cortex in control subjects. Thus, VEFs clearly demonstrated that almost all of the optic nerve axons were connected to the contralateral hemisphere of the brain in these three cases of albinism who had no visual field defect. The isofield maps with one dipole pattern demonstrated functional evidence for the misrouting of optic nerve fiber projection in the patient with albinism. We further noted that the direction of the current dipoles was different in the oculocutaneous albinism (Cases 1 and 2) from that of the ocular albinism (Case 3). This may suggest a further difference in the primary visual cortex in these two types of albinism. We are examining additional patients with albinism to determine the reliability of VEFs.

Acknowledgements

We thank Yaeko Takagi for grateful cooperation with MRI. We thank Professors Eberhart Zrenner and Yutaka Fukuda for suggestions to the manuscript.

References

Apkarian, P. (1992). A practical approach to albino diagnosis. VEP misrouting across the age span. *Ophthalmic Paediatrics and Genetics, 13*, 77–88.

Apkarian, P., Reits, D., Spekreijse, H., & Van Dorp, D. (1983). A decisive electrophysiological test for human albinism. *Electroencephalography and Clinical Neurophysiology, 55*, 513–531.

Barth, D. S., Sutherling, W., Engel, J., Jr., & Beatty, J. (1982). Neuromagnetic localization of epileptiform spike activity in the human brain. *Science, 218*, 891–894.

Bouzas, E. A., Caruso, R. C., Drews-Bankiewicz, M. A., & Kaiser-Kupfer, M. I. (1994). Evoked potential analysis of visual pathways in human albinism. *Ophthalmology, 101*, 1867–1868.

Carroll, W. M., Jay, B. S., McDonald, W. I., & Halliday, A. M. (1980). Pattern evoked potentials in human albinism. Evidence of two different topographical asymmetries reflecting abnormal retino-cortical projections. *Journal of Neurological Sciences, 48*, 265–286.

Cohen, D. (1972). Magnetoencephalography: Detection of the brain's electrical activity with a superconducting magnetometer. *Science, 175*, 664–666.

Creel, D. J. (1971). Visual system anomaly associated with albinism in the cat. *Nature, 231*, 465–466.

Creel, D. J. (1978). Visual system anomalies in human ocular albinos. *Science, 201*, 931–933.

Creel, D. J., Witkop, C. J., & King, R. A. (1974). Asymmetric visually evoked potentials in human albinos: Evidence for visual system anomalies. *Investigative Ophthalmology and Visual Science, 13*, 430–440.

Fizgerald, K., & Cibis, G. W. (1994). The value of flash visual evoked potentials in albinism. *Journal of Pediatric Ophthalmology and Strabismus, 31*, 18–25.

Gross, K. J., & Hickey, T. L. (1980). Abnormal laminar patterns in the lateral geniculate nucleus of an albino monkey. *Brain Research, 190*, 231–237.

Guillery, R. W., & Kaas, J. H. (1973). Genetic abnormality of visual pathways in a 'white' tiger. *Science, 180*, 1287–1289.

Guillery, R. W., Okoro, A. N., & Witkop, C. J. (1975). Abnormal visual pathways in the brain of a human albino. *Brain Research, 96*, 373–377.

Hatanaka, K., Nakasato, N., Seki, K., Kanno, A., Mizoi, K., & Yoshimoto, T. (1997). Striate cortical generators of the N75, P100 and N145 components localized by pattern reversal visual evoked magnetic fields. *Tohoku Journal of Experimental Medicine, 182*, 9–14.

Hedera, P., Lai, S., Haacke, E. M., Lerner, A. J., Hopkins, A. L., Lewin, J. S., & Friedland, R. P. (1994). Abnormal connectivity of the visual pathways in human albinos demonstrated by susceptibility-sensitized MRI. *Neurology, 44*, 1921–1926.

Lund, R. D. (1965). Uncrossed visual pathways of hooded and albino rats. *Science, 149*, 1506–1507.

McHam, M. L., & Fulton, A. (1992). Albinism. *International Ophthalmology Clinics, 32*, 185–200.

Morland, A. B., Hoffmann, M. B., Neveu, M., & Holder, G. E. (2002). Abnormal visual projection in a human albino studied with functional magnetic resonance imaging and visual evoked potentials. *Journal of Neurology Neurosurgery and Psychiatry, 72*, 523–526.

Nakagawa, Y., Kiyosawa, M., Tamai, M., & Ito, M. (1993). Positron emission tomography and 18F-fluorodeoxyglucose for the detection of visual pathway abnormalities in albinism. *American Journal of Ophthalmology, 116*, 112–113.

Nakasato, N., Seki, K., Fujita, S., Hatanaka, K., Kawamura, T., Ohtomo, S., Kanno, A., Ikeda, H., & Yoshimoto, T. (1996). Clinical application of visual evoked fields using an MRI-linked whole head MEG system. *Frontiers of Medical and Biological Engineering, 7*, 275–283.

Oguchi, Y. (1998). Visual information processing and the mechanism of vision. Clinical application. *Nippon Ganka Gakkai Zasshi, 102*, 850–875.

Russell-Eggitt, I., Kriss, A., & Taylor, D. S. (1990). Albinism in childhood: A flash VEP and ERG study. *British Journal of Ophthalmology, 74*, 136–140.

Sanderson, K. J. (1975). Retinogeniculate projections in the rabbits of the albino allelomorphic series 1. *Journal of Comparative Neurology, 159*, 15–27.

Seki, K., Nakasato, N., Fujita, S., Hatanaka, K., Kawamura, T., Kanno, A., & Yoshimoto, T. (1996). Neuromagnetic evidence that the P100 component of the pattern reversal visual evoked response originates in the bottom of the calcarine fissure. *Electroencephalography and Clinical Neurophysiology, 100*, 436–442.

Soong, F., Levin, A. V., & Westall, C. A. (2000). Comparison of techniques for detecting visually evoked potential asymmetry in albinism. *Journal of AAPOS, 4*, 302–331.

Selective Suppression of Pathologic, but Not Physiologic, Retinal Neovascularization by Blocking the Angiotensin II Type 1 Receptor

Norihiro Nagai,[1,2] Kousuke Noda,[1] Takashi Urano,[2] Yoshiaki Kubota,[2] Hajime Shinoda,[1,3] Takashi Koto,[1,3] Kei Shinoda,[1] Makoto Inoue,[1] Takayuki Shiomi,[3] Eiji Ikeda,[3] Kazuo Tsubota,[1] Toshio Suda,[2] Yuichi Oike,[2] and Susumu Ishida[1]

Purpose. To investigate the anti-inflammatory and anti-angiogenic effects of telmisartan, an angiotensin II type 1 receptor (AT1-R) antagonist, on ischemia-induced retinal neovascularization.

Methods. C57BL/6 neonatal mice were reared in an 80% concentration of oxygen from postnatal day (P)7 to P12, followed by room-air breathing until P17, to induce ischemia-initiated retinal neovascularization (i.e., a murine model of ischemic retinopathy). Tissue localization of AT1-R was examined by immunohistochemistry for murine retinal wholemounts and human fibrovascular tissues excised at vitrectomy for proliferative diabetic retinopathy. Animals received intraperitoneal injection of telmisartan or vehicle. A concanavalin A lectin perfusion-labeling technique was used to evaluate the areas of physiological and pathologic retinal new vessels and the number of leukocytes adhering to the vasculature. Retinal mRNA and protein levels of intercellular adhesion molecule (ICAM)-1, vascular endothelial growth factor receptor (VEGFR)-1, and VEGFR-2 were examined by RT-PCR and ELISA.

Results. Vessels in human fibrovascular tissues and the murine retinas were positive for AT1-R. Pathologic ($P < 0.01$), but not physiologic ($P > 0.05$), retinal neovascularization was significantly suppressed in telmisartan-treated mice compared with vehicle-treated animals. The number of adherent leukocytes ($P < 0.01$) was also significantly reduced, together with retinal ICAM-1 levels ($P < 0.01$) in the telmisartan-treated group compared with the control group. No significant difference was detected in retinal VEGFR-2 levels between the two groups, whereas retinal VEGFR-1 levels in the telmisartan-treated group were significantly ($P < 0.05$) lower than in the vehicle-treated group.

Conclusions. The present findings suggest that the AT1-R signaling blockade leads to the selective suppression of pathologic, but not physiological, retinal neovascularization through the inhibition of the inflammatory processes related to pathologic neovascularization. (*Invest Ophthalmol Vis Sci.* 2005;46: 1078–1084) DOI:10.1167/iovs.04-1101

The renin-angiotensin system is well known as a major controller of systemic blood pressure. Angiotensin II (Ang II), a final product of the system, has two cognate receptors: the angiotensin II type 1 receptor (AT1-R) and the angiotensin II type 2 receptor (AT2-R).[1–4] Because major Ang II-related systemic functions are mediated by AT1-R signaling, its antagonist is widely used for the treatment of hypertension and cardiac diseases. In contrast, several reports have recently suggested that Ang II plays crucial roles in promoting tumor angiogenesis and cardiovascular remodeling through the proliferation of smooth muscle cells and the induction of various growth factors.[5–16] As concerns its relationship with ocular angiogenesis, angiotensin converting enzyme inhibitor has been shown to suppress the progression of human diabetic retinopathy to its proliferative (angiogenic) stage.[17] A recent report has indicated that an AT1-R antagonist suppressed retinal neovascularization in a murine model of ischemic retinopathy[7] and supports the result of the clinical trial. However, little is known about the mechanisms of the anti-angiogenic effects of AT1-R inhibition in retinal disorders.

Retinal neovascularization is a hallmark of vision-threatening retinal diseases, including diabetic retinopathy and retinopathy of prematurity, which are major causes of blindness in adults and children, respectively. There are two distinctly different types of retinal neovascularization, physiological versus pathologic, both of which are basically induced by retinal ischemia. In the former, new vessels grow systematically in the retina to compensate for the retinal ischemia, whereas in the latter, retinal new vessels ectopically invade the transparent vitreous, which originally lacks the vasculature. Because simultaneous prevention of both types of retinal neovascularization causes retinal ischemia to be untreated, ophthalmologists await the establishment of new therapy that selectively targets pathologic neovascularization, while sparing compensatory physiological neovascularization. We have recently highlighted the molecular and cellular mechanisms differentiating pathologic from physiological retinal neovascularization.[18–20] The influx of inflammatory cells at the growing tip of new vessels is likely to be a critical step of changing the direction of retinal neovascularization from intraretinal to extraretinal growth.

Recent reports have suggested that Ang II plays a key role in various inflammatory processes, including not only the expression of chemokines and adhesion molecules for the recruitment of inflammatory cells, but also the differentiation and proliferation of inflammatory cells, per se.[21–24] Blockade of Ang II signaling seems to be a useful strategy for the improvement of inflammation-related diseases. Focusing on the inflammatory mechanisms that promote pathologic, but not physiological, retinal neovascularization, we investigated the differential effects of an AT1-R antagonist, telmisartan, on each

From the Departments of [1]Ophthalmology, [2]Cell Differentiation, and [3]Pathology, Keio University School of Medicine, Tokyo, Japan.

Submitted for publication September 16, 2004; revised November 7, 2004; accepted November 24, 2004.

Disclosure: **N. Nagai**, Boehringer Ingelheim (F); **K. Noda**, Boehringer Ingelheim (F); **T. Urano**, None; **Y. Kubota**, None; **H. Shinoda**, Boehringer Ingelheim (F); **T. Koto**, Boehringer Ingelheim (F); **K. Shinoda**, Boehringer Ingelheim (F); **M. Inoue**, Boehringer Ingelheim (F); **T. Shiomi**, None; **E. Ikeda**, None; **K. Tsubota**, Boehringer Ingelheim (F); **T. Suda**, None; **Y. Oike**, None; **S. Ishida**, None

The publication costs of this article were defrayed in part by page charge payment. This article must therefore be marked "*advertisement*" in accordance with 18 U.S.C. §1734 solely to indicate this fact.

Corresponding author: Susumu Ishida, Department of Ophthalmology, Keio University School of Medicine, 35 Shinanomachi, Shinjuku-ku, Tokyo 160-8582, Japan; ishidasu@sc.itc.keio.ac.jp.

Investigative Ophthalmology & Visual Science, March 2005, Vol. 46, No. 3

type of retinal neovascularization in a murine model of ischemic retinopathy.

METHODS

Murine Model of Ischemic Retinopathy

C57BL/6 mice (SLC, Shizuoka, Japan) were used. All animal experiments were conducted in accordance with the ARVO Statement for the Use of Animals in Ophthalmic and Vision Research. The ethics committee of our institution approved all surgical interventions and animal care procedures, which were in accordance with the Guidelines and Policies for Animal Surgery provided by the Animal Study Committees of the Central Institute for Experimental Animals of Keio University. Postnatal day (P)7 mice with their nursing mothers were maintained for a full 5 days in 80% oxygen to generate the nonvascular retinal area, as described previously.[25] On P12, they were placed in normoxia for an additional 5 days to induce retinal neovascularization.

Intraperitoneal Injection of Telmisartan

After 80% oxygen exposure, pups were categorized into three groups: The first had no treatment (ischemic retinopathy) and the other two received 0.1-mL intraperitoneal injections of vehicle or telmisartan for 5 days in normoxia (21% oxygen) after the hyperoxic exposure (P12–P16). Telmisartan was a gift of Boehringer Ingelheim (Ingelheim, Germany). We dissolved telmisartan in dimethyl sulfoxide (DMSO) in 30 mM diluted to 60 μM with phosphate-buffered saline (PBS) and injected at 3 μg/g body weight. This dose was sufficient to block AT1-R signaling to decrease systemic blood pressure in rats.[26] The degree of retinal neovascularization and the number of adherent leukocytes were evaluated on P17.

Lectin Labeling of Retinal Vasculature and Adherent Leukocytes

The retinal vasculature and adherent leukocytes were imaged by perfusion-labeling with fluorescein-isothiocyanate (FITC)–coupled concanavalin A lectin (Con A; Vector, Burlingame, CA), as described previously.[27] After deep anesthesia, the chest cavity was opened and a 27-gauge cannula was introduced into the left ventricle. After injection of 2 mL of PBS to remove erythrocytes and nonadherent leukocytes, 2 mL FITC-conjugated con A lectin was perfused. After the eyes were enucleated, the retinas were flatmounted. The flatmounts were imaged by an epifluorescence microscope (IX71; Olympus, Tokyo, Japan), and the total number of Con A–stained adherent leukocytes per retina was determined.

Immunohistochemistry for AT1-R

Immunohistochemical experiments were performed on fibrovascular tissues from patients with diabetic retinopathy and on retinas of C57BL/6 mice. Fibrovascular tissue samples were obtained during vitrectomy performed at Keio University Hospital on patients with proliferative diabetic retinopathy, who gave their informed consent to our study. The protocol of the study adhered to the tenets of the Declaration of Helsinki regarding research involving human tissue. For histopathologic evaluation, the specimen was fixed with 4% paraformaldehyde (PFA) at 4°C immediately after removal, and embedded in paraffin.

Three-micrometer paraffin-embedded sections were incubated overnight at 4°C with a rabbit polyclonal antibody against human AT1-R (Santa Cruz Biotechnology, Santa Cruz, CA) at 1:100 dilution. After incubation, they were reacted for 30 minutes at room temperature with goat antibodies against rabbit immunoglobulins (IgGs) conjugated to a peroxidase-labeled dextran polymer (En Vision+ rabbit; Dako Corp., Carpinteria, CA). As the negative control for staining, the first antibodies were replaced with nonimmune rabbit IgGs (Dako Corp.). Color was developed with 3,3′-diaminobenzidine tetrahydrochloride (DAB; 0.2 mg/mL; Dojindo Laboratories, Kumamoto, Japan) in 0.05 M Tris-HCl (pH 7.6) containing 0.003% hydrogen peroxide, and the sections were counterstained with hematoxylin.

Wholemount retinas from P5 mice were fixed with 4% PFA and incubated overnight at 4°C with rat polyclonal antibody against platelet endothelial cell adhesion molecule-1 (PECAM-1, CD31; BD Microbiology, Cockeysville, MD) at 1:500 dilution and rabbit polyclonal antibody against human AT1-R (Santa Cruz Biotechnology) at 1:50 dilution. Avidin-Alexa 488–and Avidin-Alexa 546–tagged secondary antibody (Molecular Probes, Eugene, OR) were then applied for 2 hours at room temperature. After two washes, retinas were viewed with an epifluorescence microscope (model IX71; Olympus).

RT-PCR for Intercellular Adhesion Molecule-1 and Vascular Endothelial Growth Factor Receptor-1 and -2

Total RNA was isolated from the retina using extraction reagent (Isogen; Nippon Gene, Toyama, Japan) and reverse-transcribed with a cDNA synthesis kit (First-Strand; Pharmacia Biotech, Uppsala, Sweden) according to the manufacturers' protocols. PCR was performed with *Taq* DNA polymerase (Toyobo, Tokyo, Japan) in a thermal controller (MiniCycler; MJ Research, Watertown, MA). The primer sequences are as follows: 5′-ATG TGG CAC CAC ACC TTC TAC AAT GAG CTG CG-3′ (sense) and 5′-CGT CAT ACT CCT GCT TGC TGA TCC ACA TCT GC-3′ (antisense; 37 bp) for β-actin, 5′-GTG TCG AGC TTT GGG ATG GTA-3′ (sense) and 5′-CTG GGC TTG GAG ACT CAG TG-3′ (antisense; 505 bp) for mouse intercellular adhesion molecule (ICAM)-1. Human/mouse vascular endothelial growth factor receptor-1 (VEGF R1) primers (302 bp; PCR Primer Pair; R&D Systems, Inc., Minneapolis, MN) and human/mouse VEGF R2 primers (569 bp; PCR Primer Pair; R&D Systems, Inc.) were used for VEGFR-1 and -2, respectively.

ELISA for ICAM-1 and VEGFR-1 and -2

The animals were killed with an overdose of anesthesia, and the eyes were immediately enucleated. The retina was carefully isolated and placed into 200 μL lysis buffer (0.02 M HEPES, 10% glycerol, 10 mM $Na_4P_2O_7$, 100 μM Na_3VO_4, 1% Triton, 100 mM NaF, 4 mM EDTA [pH 8.0]) supplemented with protease inhibitors and sonicated. The lysate was centrifuged at 15,000 rpm for 15 minutes at 4°C, and the ICAM-1 and VEGFR-1 and -2 levels in the supernatant were determined with mouse ICAM-1 and VEGFR-1 and -2 kits (Techne Corp., Minneapolis, MN) according to the manufacturer's protocol. The tissue sample concentration was calculated from a standard curve and corrected for protein concentration.

Morphometric and Statistical Analyses

All results are expressed as the mean ± SD. The number of leukocytes in each flat mount was counted independently by two investigators under the epifluorescence microscope. Area ratios of pathologic and physiological neovascularization to the flatmounted retina were measured and calculated. The morphology of the pathologic neovascularization was readily discerned from the intraretinal extension of physiological vessels. The results were processed for statistical analyses (Mann-Whitney test). Differences were considered statistically significant at $P < 0.05$.

RESULTS

Localization of AT1-R in the Murine Retina and Human Fibrovascular Tissues

Immunohistochemistry for AT1-R was performed to identify its expression on the fibrovascular tissues of patients with proliferative diabetic retinopathy and on the murine retina. In the fibrovascular tissues, the vascular endothelium was positive for AT1-R (Figs. 1A, 1B). In the retina of neonatal mice, the AT1-R immunoreactivity was detected mainly on the endothelial cells of inner retinal vessels (Figs. 1C, 1D). Immunohistochemistry

FIGURE 1. Immunohistochemical staining for AT1-R. (A, B) Fibrovascular tissue of eyes with proliferative diabetic retinopathy. Most vascular endothelial cells in the fibrovascular tissue were positive for AT1-R (A, *arrows*), whereas the immunoreactivity was diminished in the negative control section (B), where the primary antibodies were replaced with nonimmune rabbit IgG. (C, D) Retinal section of a normal mouse. Positive staining for AT1-R on the inner retinal vessels (C, *arrows*). No staining appeared in the serial section for the negative control (D). (E–G) Flatmounts of neonatal mouse retinas. *Red* fluorescence from the anti-PECAM-1 antibody (E) and *green* fluorescence from the anti-AT1-R antibody (F) identified the AT1-R-positive cells as being PECAM-1-positive endothelial cells when the images were superimposed (G). Scale bars: (A, B) 25 μm; (C, D) 80 μm.

of wholemount retinas also showed AT1-R staining on retinal vessels, corresponding to the staining of PECAM-1, which is widely used as a marker of vascular endothelial cells (Figs. 1E–G).

Effects of Telmisartan on Pathologic Retinal Neovascularization and Inflammation

The retinal vasculature and adherent leukocytes were imaged by perfusion-labeling with FITC-coupled Con A. In normal P17 mice, the retina was covered with physiological (intraretinal) new vessels (Fig. 2A). In P17 mice with ischemic retinopathy, physiological new vessels and pathologic vascular buds (*arrows*) were both observed (Fig. 2B). In higher magnification, abundant leukocytes adhered to the physiological vascular bed (Fig. 2C) and pathologic neovascular fronds (Fig. 2D). Compared with vehicle-treated mice (Fig. 2E), systemic application of telmisartan led to the suppression of pathologic neovascularization on P17 (Fig. 2F). The area ratio of pathologic neovascularization in the telmisartan group was 3.2% ± 1.8%, which was significantly ($P < 0.01$) decreased compared with the vehicle group (9.7% ± 1.2%) or the ischemic retinopathy group (8.9% ± 1.3%, Fig. 3A). The number of adherent leukocytes in ischemic retinopathy (57.8 ± 16.5) was significantly ($P < 0.01$) higher than in normal P17 mice (7.8 ± 4.3, Fig. 3B). Leukocyte counts showed a significant ($P < 0.01$) decrease in the telmisartan group (21.3 ± 7.0), compared with the vehicle group (53.7 ± 9.4) or the nontreated ischemic retinopathy group (57.8 ± 16.5, Fig. 3B).

Effects of Telmisartan on Physiological Retinal Neovascularization

Area ratios of physiological neovascularization in ischemic retinopathy were compared among nontreated, vehicle- and telmisartan-treated groups (Figs. 2B, 2E, 2F). No significant ($P > 0.05$, Fig. 4A) difference was detected in physiological neovascularization area between the telmisartan group (62.7% ± 3.7%) and the vehicle group (55.2% ± 5.7%) or the nontreated retinopathy group (69.9% ± 4.4%). To confirm further this sparing effect of telmisartan on physiological vasculature, normal adult mice (Figs. 5A, 5B) and neonates undergoing retinal vascular development (Figs. 5C, 5D) were used . There was no morphologic difference in adult physiological vessels between vehicle-treated (Fig. 5A) and telmisartan-treated (Fig. 5B) groups. As for physiological neovascularization during postnatal retinal development, no significant ($P > 0.05$, Fig. 5B) difference was detected in physiological neovascularization area between the telmisartan group (98.8% ± 2.4%) and the

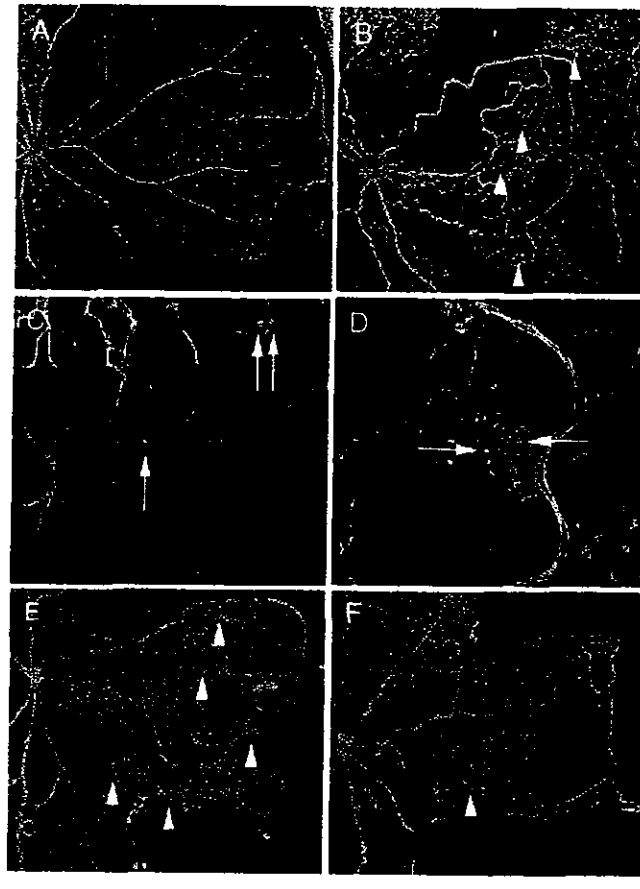

FIGURE 2. Flatmounted retinas from a P17 normal mouse (A) and a mouse with ischemic retinopathy with pathologic neovascular buds (B, *arrowheads*). (C) Adherent leukocytes (*arrows*) followed by pathologic neovascularization. (D) Adherent leukocytes (*arrows*) accompanied by pathologic neovascularization. (E) Vehicle-injected retinopathy mice showing no apparent difference in pathologic neovascularization (*arrowheads*) compared with nontreated retinopathy mice (B). (F) Telmisartan-treated retinopathy showing decreased pathologic neovascularization (*arrowheads*) and intact physiological neovascularization compared to vehicle-treated retinopathy mice (E).

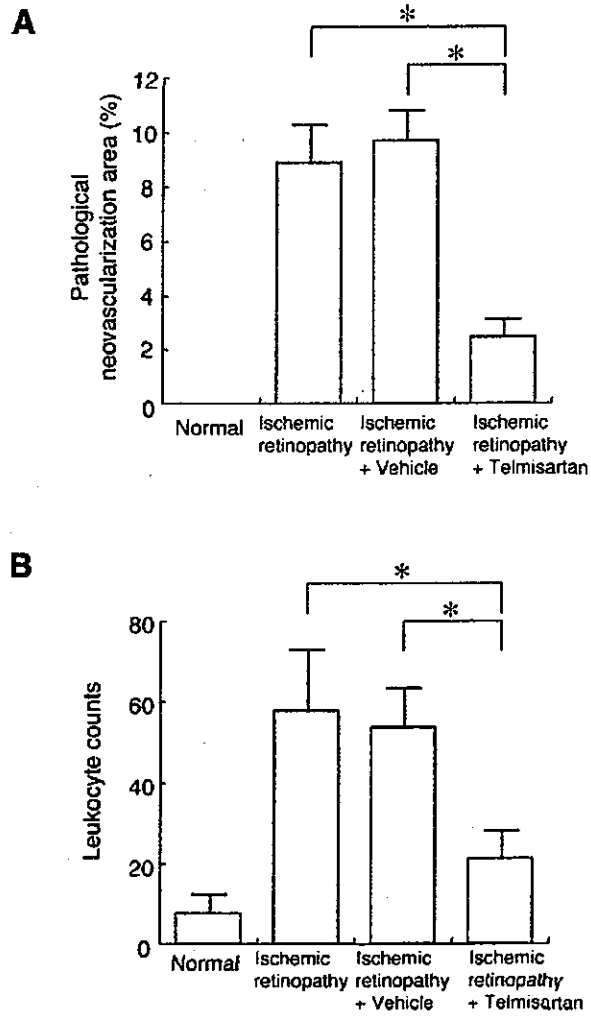

FIGURE 3. Effects of telmisartan on pathologic neovascularization (A) and inflammation (B). Telmisartan-treated mice with retinopathy showed significantly less pathologic neovascularization and significantly fewer adherent leukocytes than nontreated or vehicle-treated mice. The results represent means ± SD. *$P < 0.01$ by Mann-Whitney test.

vehicle group (99.8% ± 0.9%) or the nontreated group (99.7% ± 0.9%).

Detection of mRNA and Protein Levels Of ICAM-1 and VEGFR-1 and -2

Retinas from P17 mice were subjected to RT-PCR and ELISA analyses to detect the mRNA and protein levels of ICAM-1, VEGFR-1, and VEGFR-2 (Fig. 6). Retinal ICAM-1 mRNA levels in ischemic retinopathy treated with vehicle were higher than in normal age-matched mice. Systemic administration of telmisartan substantially reduced ICAM-1 mRNA levels (Fig. 6A). Similarly, retinal ICAM-1 protein levels were significantly attenuated by the treatment with telmisartan ($P < 0.01$, Fig. 6B). Retinal VEGFR-1 mRNA and protein levels in vehicle-treated mice with retinopathy tended to increase compared with those in normal age-matched mice, but the difference was not statistically significant ($P > 0.05$). Telmisartan treatment for ischemic retinopathy significantly attenuated both mRNA and protein levels of retinal VEGFR-1 ($P < 0.05$; Figs. 6A, 6C). In contrast, there was no difference in retinal VEGFR-2 mRNA or protein levels among normal age-matched mice and the vehicle-, and telmisartan-treated retinopathy mice ($P > 0.05$, Figs. 6A, 6D).

DISCUSSION

The present study demonstrates for the first time that AT1-R blockade selectively prevents pathologic retinal neovascularization, while sparing physiological neovascularization that compensates for the preceding retinal ischemia. Furthermore, we showed that the mechanisms in the differential modulation of retinal neovascularization depend, at least in part, on the suppression of ICAM-1-mediated leukocyte adhesion to the retinal vasculature, inflammatory processes that characterize pathologic retinal neovascularization.

We have proposed that ischemia-induced retinal neovascularization, when it becomes pathologic, involves inflammatory processes.[18–20] A previous immunohistochemical study pointed out the infiltration of macrophages in fibrovascular tissues excised at vitrectomy for proliferative diabetic retinop-

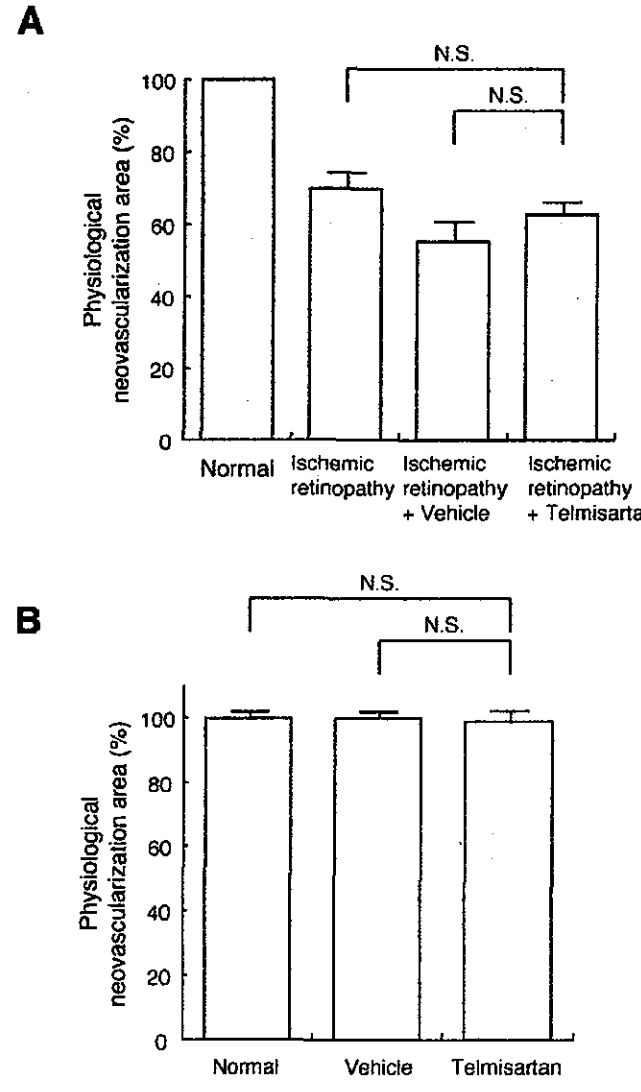

FIGURE 4. Effects of telmisartan on physiological neovascularization in ischemic retinopathy (A) and during normal vascular development (B). Telmisartan-treated mice exhibited no significant difference in physiological neovascularization compared with vehicle-treated or nontreated mice. The results represent means ± SD. *$P < 0.01$ by Mann-Whitney test.

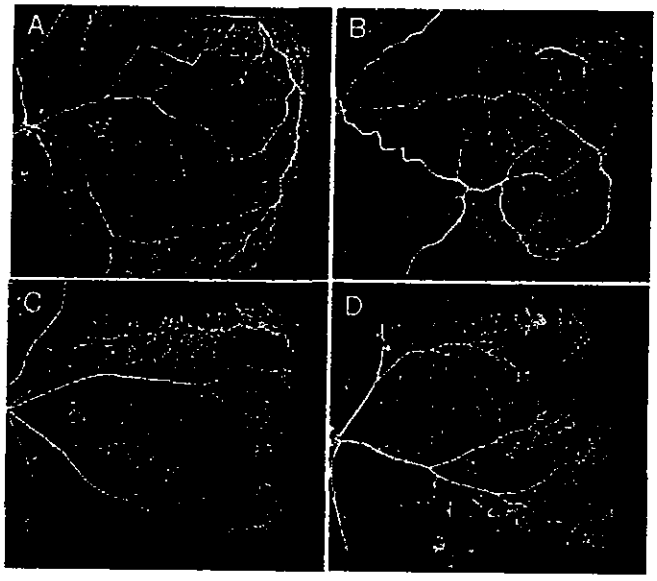

FIGURE 5. Flatmounted retinas from normal adult mice (A, B) and neonates with physiological vascular development (C, D). No morphologic difference was detected between vehicle-treated (A, C) and telmisartan-treated mice (B, D).

athy,[28] indicating a possible link between retinal neovascularization and inflammation. In an animal model of ischemic retinopathy, pathologic, but not physiological, neovascularization was shown to be preceded and accompanied by the adhesion of inflammatory monocytes to the retinal vasculature. When clodronate-liposome, a reagent that induces apoptosis specifically in monocyte/macrophage cells, was used, pathologic retinal neovascularization was suppressed without any substantial effects on physiological neovascularization.[18] In addition, other reports have suggested the proangiogenic role of inflammatory monocytes and macrophages in murine ischemic retinopathy. Intravitreally infiltrating macrophages adjacent to the pathologic new vessels express and produce VEGF in the animal model.[29] Neutralizing antibodies against monocyte chemotactic protein (MCP)-1 and macrophage inflammatory protein (MIP)-1α have been shown to reduce pathologic retinal neovascularization and inflammation.[30] Therefore, inflammatory monocytes are likely to disrupt the direction of physiological neovascularization, triggering pathologic retinal neovascularization.

ICAM-1 is a ligand for β2-integrins constitutively expressed on the leukocyte surface and is a key adhesion molecule that controls leukocyte adhesion to the vessel walls.[31] ICAM-1, constitutively expressed on vascular endothelial cells at a low level, is swiftly upregulated during inflammation, resulting in enhancement of leukocyte-endothelial interaction. A previous study in donor eyes demonstrated that diabetic retinas had increased levels of ICAM-1 immunoreactivity in the vessels as well as infiltrating leukocytes, compared with normal retinas.[32] In a rodent model of diabetes, ICAM-1-dependent leukocyte adhesion is enhanced in the early stage,[33,34] and various retinal diseases related to long-term diabetes have been shown to be mediated by ICAM-1.[35] In vitro, Ang II was shown to induce the expression of ICAM-1 on vascular endothelial and promote leukocyte-endothelial adhesion.[22] In accordance with the in

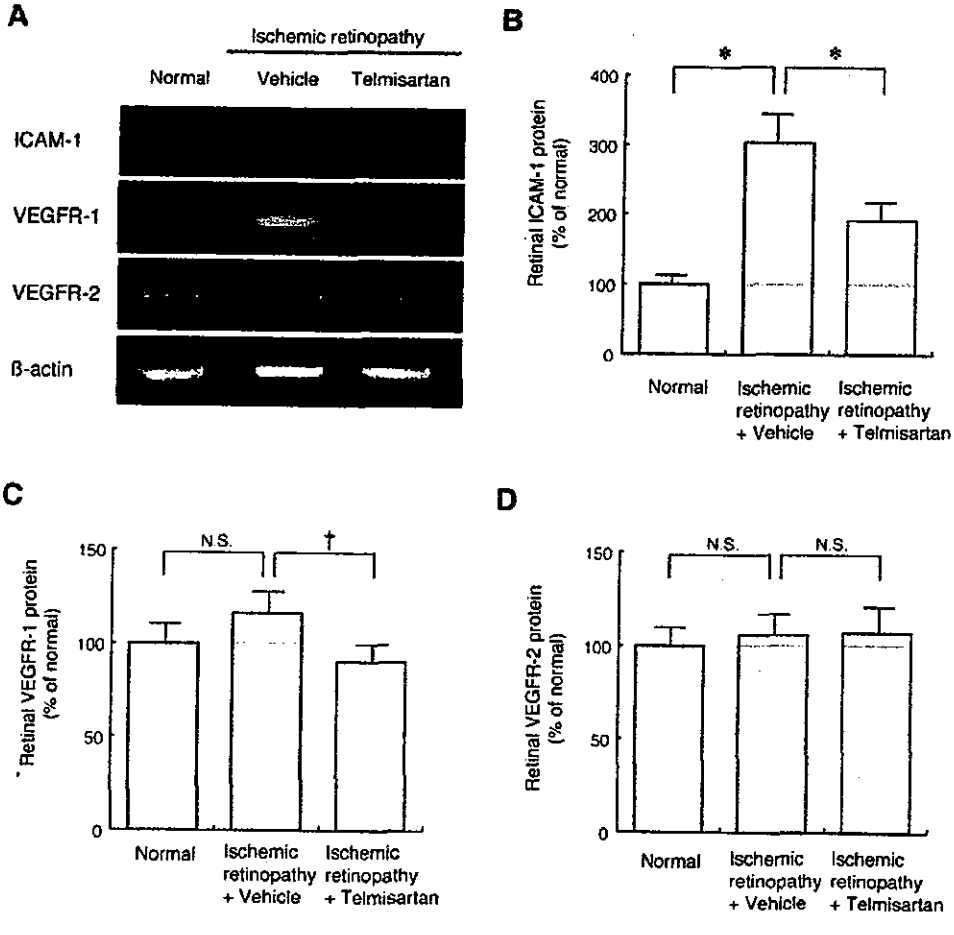

FIGURE 6. RT-PCR (A) and ELISA (B, C) analyses for retinal ICAM-1 and VEGFR-1 and -2. (A) Retinal ICAM-1 mRNA expression in ischemic retinopathy treated with telmisartan, reduced to those in normal mice, was lower than those in vehicle-treated mice with retinopathy. Retinal VEGFR-1 mRNA expression in telmisartan-treated retinopathy mice also decreased compared with vehicle-treated mice with retinopathy. There was no apparent difference in retinal VEGFR-2 expression between vehicle-treated and telmisartan-treated mice. (B) Retinal ICAM-1 protein levels in vehicle-treated mice with retinopathy were significantly higher than in normal mice and were significantly suppressed by treatment with telmisartan. The results are expressed as the mean ± SD; $n = 6$. $^*P < 0.01$ by Mann-Whitney test. (C) Retinal VEGFR-1 protein levels in telmisartan-treated mice with retinopathy were significantly lower than in vehicle-treated mice with retinopathy; $n = 6$. $\dagger P < 0.05$. (D) No significant ($P > 0.05$) difference in retinal protein levels of VEGFR-2 was detected among three groups ($n = 6$).

vitro data, telmisartan-treated animals in our study exhibited the decreased retinal ICAM-1 mRNA and protein expression as well as the suppressed leukocyte adhesion to the retinal vessels, reasonably resulting in the inhibition of inflammation-related pathologic neovascularization.

As for other proangiogenic mechanisms shown in the literature, Ang II induced the in vitro expression of VEGFR-2 mRNA on cultured bovine retinal endothelial cells and pericytes, enhancing VEGF-induced angiogenic activity.[15,16] VEGF has two cognate receptors called VEGFR-1 and -2.[36–38] VEGF-mediated endothelial cell mitogenic activity was shown to depend, not on VEGFR-1, but on VEGFR-2.[39] In our ischemic retinopathy model, as others reported,[40] retinal VEGFR-2 expression showed levels similar to those in retinal vascular development, and telmisartan had a minimal effect on VEGFR-2 expression levels in vivo. Although VEGFR-2 blockade in the retinopathy model was reported to result in the suppression of pathologic neovascularization,[40] the telmisartan-induced effects shown in the present study are thought to be mediated, not by VEGFR-2 inhibition, but mainly by ICAM-1 inhibition, causing the prevention of inflammation to maintain the right direction of physiological neovascularization.

The current data show that AT1-R blockade led to the significant decrease in retinal VEGFR-1 levels in ischemic retinopathy. Shih et al.[41] showed that VEGFR-1 signaling activated by placental growth factor (PlGF)-1 led to the suppression of hyperoxia-induced vaso-obliteration and suggested the possibility of VEGFR-1-mediated prevention of pathologic retinal neovascularization secondary to the decreased extent of retinal ischemia. They also described that PlGF-activated signaling of VEGFR-1 did not affect any of three types of vaso-proliferation (i.e., physiological neovascularization during normal retinal development, physiological neovascularization after hyperoxia-induced ischemia, or pathologic neovascularization after hyperoxia-induced ischemia). In the present study, we applied telmisartan to mice with retinopathy during the proliferative stage after the phase of hyperoxia-induced vaso-obliteration. Reasonably, our administration of telmisartan did not affect the extent of avascular area formation in these mice. Because vasoproliferation after the ischemic phase depends not on VEGFR-1,[41] but on VEGFR-2,[40] VEGFR-1 downregulation on vascular endothelial cells is thought to have little or no effect on retinal neovascularization. In contrast, VEGFR-1 is well-known to be expressed on inflammatory leukocytes including monocytes.[42–44] The telmisartan-induced decrease in retinal VEGFR-1 seen in the present study, therefore, is compatible with and explained at least in part by the suppression of VEGFR-1-bearing inflammatory leukocytes' adhering to the retinal vasculature.

Although in a recent paper the antiangiogenic effect of AT1-R blockade (losartan) on pathologic retinal neovascularization in ischemic retinopathy was reported,[7] no comparison was made between physiological versus pathologic neovascularization, and no mechanistic explanation was provided about the inhibitory effects on pathologic neovascularization. In this context, the present study is the first to indicate the molecular and cellular mechanisms in the differential effects of AT1-R blockade on both types of retinal neovascularization. Our novel findings are supported by a recent paper showing that Ang II-mediated subcutaneous neovascularization in a murine model (Matrigel; BD Biosciences, Franklin Lakes, NJ) is mediated by inflammation-related pathways.[6]

Currently, several AT1-R antagonists are widely applied to hypertensive patients and have been shown to be safe and effective.[45,46] Hypertension is well known to be a worsening factor in proliferative diabetic retinopathy.[47] A recent report[48] has shown the increased levels of Ang II in the vitreous fluid of patients with proliferative diabetic retinopathy, although its role in pathogenesis remains undetermined. More work is needed to establish the validity of this therapeutic approach in vision-threatening ischemic retinopathies.

References

1. de Gasparo M, Catt KJ, Inagami T, Wright JW, Unger T. International union of pharmacology. XXIII. The angiotensin II receptors. *Pharmacol Rev.* 2000;52:415–472.
2. de Gasparo M, Husain A, Alexander W, et al. Proposed update of angiotensin receptor nomenclature. *Hypertension.* 1995;25:924–927.
3. Murphy TJ, Alexander RW, Griendling KK, Runge MS, Bernstein KE. Isolation of a cDNA encoding the vascular type-1 angiotensin II receptor. *Nature.* 1991;351:233–236.
4. Sasaki K, Yamano Y, Bardhan S, et al. Cloning and expression of a complementary DNA encoding a bovine adrenal angiotensin II type-1 receptor. *Nature.* 1991;351:230–233.
5. Tamarat R, Silvestre JS, Durie M, Levy BI. Angiotensin II angiogenic effect in vivo involves vascular endothelial growth factor- and inflammation-related pathways. *Lab Invest.* 2002;82:747–756.
6. Moravski CJ, Kelly DJ, Cooper ME, et al. Retinal neovascularization is prevented by blockade of the renin-angiotensin system. *Hypertension.* 2000;36:1099–1104.
7. Lonchampt M, Pennel L, Duhault J. Hyperoxia/normoxia-driven retinal angiogenesis in mice: a role for angiotensin II. *Invest Ophthalmol Vis Sci.* 2001;42:429–432.
8. Fujita M, Hayashi I, Yamashina S, Itoman M, Majima M. Blockade of angiotensin AT1a receptor signaling reduces tumor growth, angiogenesis, and metastasis. *Biochem Biophys Res Commun.* 2002;294:441–447.
9. Miyajima A, Kosaka T, Asano T, et al. Angiotensin II type I antagonist prevents pulmonary metastasis of murine renal cancer by inhibiting tumor angiogenesis. *Cancer Res.* 2002;62:4176–4179.
10. Walsh DA, Hu DE, Wharton J, Catravas JD, Blake DR, Fan TP. Sequential development of angiotensin receptors and angiotensin I converting enzyme during angiogenesis in the rat subcutaneous sponge granuloma. *Br J Pharmacol.* 1997;120:1302–1311.
11. Stoll M, Steckelings UM, Paul M, Bottari SP, Metzger R, Unger T. The angiotensin AT2-receptor mediates inhibition of cell proliferation in coronary endothelial cells. *J Clin Invest.* 1995;95:651–657.
12. Daemen MJ, Lombardi DM, Bosman FT, Schwartz SM. Angiotensin II induces smooth muscle cell proliferation in the normal and injured rat arterial wall. *Circ Res.* 1991;68:450–456.
13. Delafontaine P, Lou H. Angiotensin II regulates insulin-like growth factor I gene expression in vascular smooth muscle cells. *J Biol Chem.* 1993;268:16866–16870.
14. Chua CC, Hamdy RC, Chua BH. Upregulation of vascular endothelial growth factor by angiotensin II in rat heart endothelial cells. *Biochim Biophys Acta.* 1998;1401:187–194.
15. Otani A, Takagi H, Suzuma K, Honda Y. Angiotensin II potentiates vascular endothelial growth factor-induced angiogenic activity in retinal microcapillary endothelial cells. *Circ Res.* 1998;82:619–628.
16. Otani A, Takagi H, Oh H, et al. Angiotensin II-stimulated vascular endothelial growth factor expression in bovine retinal pericytes. *Invest Ophthalmol Vis Sci.* 2000;41:1192–1199.
17. Chaturvedi N, Sjolie AK, Stephenson JM, et al. Effect of lisinopril on progression of retinopathy in normotensive people with type 1 diabetes. The EUCLID Study Group. EURODIAB Controlled Trial of Lisinopril in Insulin-Dependent Diabetes Mellitus. *Lancet.* 1998;351:28–31.
18. Ishida S, Usui T, Yamashiro K, et al. VEGF164-mediated inflammation is required for pathological, but not physiological, ischemia-induced retinal neovascularization. *J Exp Med.* 2003;198:483–489.
19. Ishida S, Yamashiro K, Usui T, et al. Leukocytes mediate retinal vascular remodeling during development and vaso-obliteration in disease. *Nat Med.* 2003;9:781–788.
20. Ishida S, Usui T, Yamashiro K, et al. VEGF164 is proinflammatory in the diabetic retina. *Invest Ophthalmol Vis Sci.* 2003;44:2155–2162.

21. Hernandez-Presa M, Bustos C, Ortego M, et al. Angiotensin-converting enzyme inhibition prevents arterial nuclear factor-kappa B activation, monocyte chemoattractant protein-1 expression, and macrophage infiltration in a rabbit model of early accelerated atherosclerosis. *Circulation.* 1997;95:1532-1541.
22. Pastore L, Tessitore A, Martinotti S, et al. Angiotensin II stimulates intercellular adhesion molecule-1 (ICAM-1) expression by human vascular endothelial cells and increases soluble ICAM-1 release in vivo. *Circulation.* 1999;100:1646-1652.
23. Grafe M, Auch-Schwelk W, Zakrzewicz A, et al. Angiotensin II-induced leukocyte adhesion on human coronary endothelial cells is mediated by E-selectin. *Circ Res.* 1997;81:804-811.
24. Okamura A, Rakugi H, Ohishi M, et al. Upregulation of renin-angiotensin system during differentiation of monocytes to macrophages. *J Hypertens.* 1999;17:537-545.
25. Smith LE, Wesolowski E, McLellan A, et al. Oxygen-induced retinopathy in the mouse. *Invest Ophthalmol Vis Sci.* 1994;35:101-111.
26. Balt JC, Mathy MJ, Pfaffendorf M, van Zwieten PA. I Inhibition of angiotensin II-induced facilitation of sympathetic neurotransmission in the pithed rat: a comparison between losartan, irbesartan, telmisartan, and captopril. *J Hypertens.* 2001;19:465-473.
27. Joussen AM, Murata T, Tsujikawa A, Kirchhof B, Bursell SE, Adamis AP. Leukocyte-mediated endothelial cell injury and death in the diabetic retina. *Am J Pathol.* 2001;158:147-152.
28. Esser P, Heimann K, Wiedemann P. Macrophages in proliferative vitreoretinopathy and proliferative diabetic retinopathy: differentiation of subpopulations. *Br J Ophthalmol.* 1993;77:731-733.
29. Naug HL, Browning J, Gole GA, Gobe G. Vitreal macrophages express vascular endothelial growth factor in oxygen-induced retinopathy. *Clin Exp Ophthalmol.* 2000;28:48-52.
30. Yoshida S, Yoshida A, Ishibashi T, Elner SG, Elner VM. Role of MCP-1 and MIP-1alpha in retinal neovascularization during postischemic inflammation in a mouse model of retinal neovascularization. *J Leukoc Biol.* 2003;73:137-144.
31. Smith CW, Marlin SD, Rothlein R, Toman C, Anderson DC. Cooperative interactions of LFA-1 and Mac-1 with intercellular adhesion molecule-1 in facilitating adherence and transendothelial migration of human neutrophils in vitro. *J Clin Invest.* 1989;83:2008-2017.
32. McLeod DS, Lefer DJ, Merges C, Lutty GA. Enhanced expression of intracellular adhesion molecule-1 and P-selectin in the diabetic human retina and choroid. *Am J Pathol.* 1995;147:642-653.
33. Miyamoto K, Khosrof S, Bursell SE, et al. Prevention of leukostasis and vascular leakage in streptozotocin-induced diabetic retinopathy via intercellular adhesion molecule-1 inhibition. *Proc Natl Acad Sci USA.* 1999;96:10836-10841.
34. Joussen AM, Poulaki V, Qin W, et al. Retinal vascular endothelial growth factor induces intercellular adhesion molecule-1 and endothelial nitric oxide synthase expression and initiates early diabetic retinal leukocyte adhesion in vivo. *Am J Pathol.* 2002;160:501-509.
35. Joussen AM, Poulaki V, Le ML, et al. A central role for inflammation in the pathogenesis of diabetic retinopathy. *FASEB J.* 2004;18:1450-1452.
36. Shibuya M, Yamaguchi S, Yamane A, et al. Nucleotide sequence and expression of a novel human receptor-type tyrosine kinase gene (flt) closely related to the fms family. *Oncogene.* 1990;5:519-524.
37. Terman BI, Carrion ME, Kovacs E, Rasmussen BA, Eddy RL, Shows TB. Identification of a new endothelial cell growth factor receptor tyrosine kinase. *Oncogene.* 1991;6:1677-1683.
38. Waltenberger J, Claesson-Welsh L, Siegbahn A, Shibuya M, Heldin CH. Different signal transduction properties of KDR and Flt1, two receptors for vascular endothelial growth factor. *J Biol Chem.* 1994;269:26988-26995.
39. Ishihama H, Ohbayashi M, Kurosawa N, et al. Colocalization of neuropilin-1 and Flk-1 in retinal neovascularization in a mouse model of retinopathy. *Invest Ophthalmol Vis Sci.* 2001;42:1172-1178.
40. McLeod DS, Taomoto M, Cao J, Zhu Z, Witte L, Lutty GA. Localization of VEGF receptor-2 (KDR/Flk-1) and effects of blocking it in oxygen-induced retinopathy. *Invest Ophthalmol Vis Sci.* 2002;43:474-482.
41. Shih SC, Ju M, Liu N, Smith LE. Selective stimulation of VEGFR-1 prevents oxygen-induced retinal vascular degeneration in retinopathy of prematurity. *J Clin Invest.* 2003;112:50-57.
42. Usui T, Ishida S, Yamashiro K, et al. VEGF164(165) as the pathological isoform: differential leukocyte and endothelial responses through VEGFR1 and VEGFR2. *Invest Ophthalmol Vis Sci.* 2004;45:368-374.
43. Sawano A, Iwai S, Sakurai Y, et al. Flt-1, vascular endothelial growth factor receptor 1, is a novel cell surface marker for the lineage of monocyte-macrophages in humans. *Blood.* 2001;97:785-791.
44. Clauss M, Weich H, Breier G, et al. The vascular endothelial growth factor receptor Flt-1 mediates biological activities: implications for a functional role of placenta growth factor in monocyte activation and chemotaxis. *J Biol Chem.* 1996;271:17629-17634.
45. Neutel JM, Kolloch RE, Plouin PF, Meinicke TW, Schumacher H. OTELLOH Study Group. Telmisartan vs losartan plus hydrochlorothiazide in the treatment of mild-to-moderate essential hypertension: a randomised ABPM study. *J Hum Hypertens.* 2003;17:569-575.
46. Mallion J, Siche J, Lacourciere Y. ABPM comparison of the antihypertensive profiles of the selective angiotensin II receptor antagonists telmisartan and losartan in patients with mild-to-moderate hypertension. *J Hum Hypertens.* 1999;13:657-664.
47. UK Prospective Diabetes Study Group. Tight blood pressure control and risk of macrovascular and microvascular complications in type 2 diabetes: UKPDS 38. *BMJ.* 1998;317:703-713.
48. Funatsu H, Yamashita H, Nakanishi Y, Hori S. Angiotensin II and vascular endothelial growth factor in the vitreous fluid of patients with proliferative diabetic retinopathy. *Br J Ophthalmol.* 2002;86:311-315.

NONINVASIVE EVALUATION FOR RETINAL PIGMENT EPITHELIUM HAMARTOMA

YURI SATO, MD,
MAKOTO INOUE, MD,
NORIHIRO NAGAI, MD,
KEI SHINODA, MD,
HAJIME SHINODA, MD,
YOSHIHISA OGUCHI, MD

From the Department of Ophthalmology, Keio University School of Medicine, Tokyo, Japan.

Congenital anomalies of the retinal pigment epithelium (RPE) have been classified into four categories: RPE hamartoma, combined RPE and retinal hamartoma, melanotic nevi of the RPE (congenital hypertrophy of the RPE, or CHRPE), and amelanotic nevi of the RPE.[1] RPE hamartomas are detected typically in the temporal macular area in young adults during routine eye examination; they usually do not change in size over time.[1-4] Here we describe two cases with asymptomatic RPE hamartomas located at the central macula or the paramacula that were precisely localized and depicted by noninvasive optical coherence tomography (OCT) and scanning laser ophthalmoscope (SLO) microperimetry.

Case Report

Case 1

A 20-year-old Japanese woman was referred to us for further evaluation of a retinal "black spot" seen on funduscopy in her right eye. She had a paracentral scotoma only after the examiner had called her attention to an ophthalmoscopically evident lesion. Visual acuity was 25/20 in the affected eye. Funduscopic examination

This study received no grant support in reporting these clinical observations.

Reprint requests: Makoto Inoue, MD, Department of Ophthalmology, Keio University School of Medicine, 35 Shinanomachi, Shinjyuku, Tokyo 160-8582, Japan; e-mail: inoshin@sc.itc.keio.ac.jp

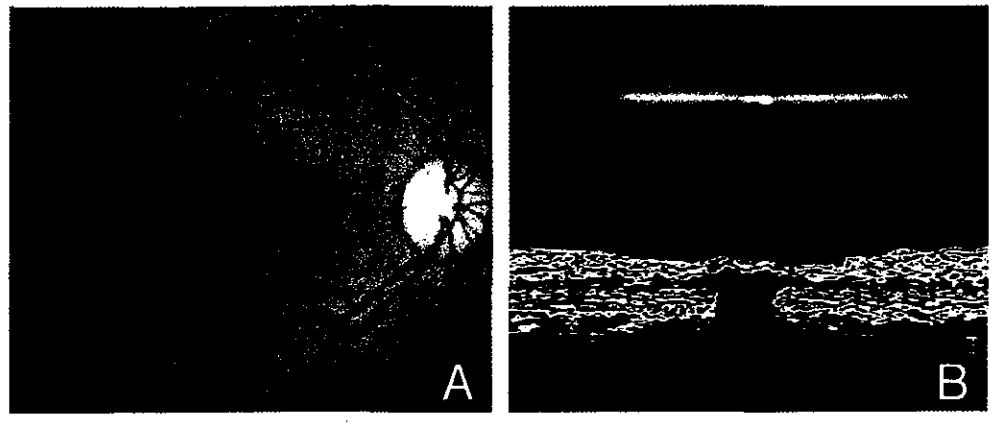

Fig. 1. Case 1. A, Fundus photograph of the right eye indicating a dark spot at the central macula. B, Optical coherence tomography (OCT) image in a horizontal section showing a highly reflected area in the superficial fovea with lack of deeper reflectivity.

revealed a round-pigmented spot at the central macula; the lesion was located just above the fovea according to a stereoptical slit-lamp examination using a contact lens (Figure 1A). The OCT image showed a highly reflected area in the superficial retina and lack of deeper reflectivity (Figure 1B). A careful search was carried out for a subjective central scotoma in the right eye, but none of the examinations, including Goldman perimetry, Humphrey visual field analyzer, and SLO microperimetry (0 dB and 20 dB; intensity at size 3), could detect any scotoma inside and around the pigmented spot (Figure 2A). Thus, the sensory retina at the area of pigmentation was found to be functional. SLO microperimetry detected the fixation point at the superonasal margin of the pigmented spot. Fluorescein angiography showed no vascular abnormality except for an area of partial obstruction of retinal fluorescence at the temporal capillary network surrounding a foveal avascular zone, indicating a superficial location of the pigmented lesion (Figure 2B).

Case 2

A 27-year-old white man was pointed out his pigmented spot in his right eye at routine examination of refractive surgery and was referred to us for further examination (Figure 3). Visual acuity was 25/20 in the affected eye. Funduscopic examination revealed an

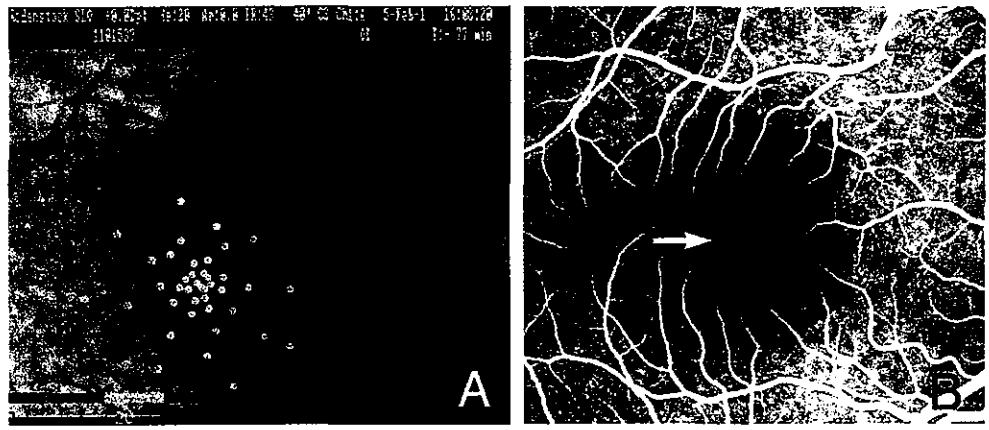

Fig. 2. Case 1. A, Detection of scotoma by 20 dB, intensity at size 3 in scanning laser ophthalmoscope (SLO) microperimetry. SLO microperimetry detects all spots, including the pigmented lesion as visible points (yellow circle figure) with no scotoma (triangle figure). B, Highly magnified photograph of fluorescein angiogram showing a partial obstruction of retinal fluorescence at the temporal capillary network surrounding a foveal avascular zone (yellow arrow).

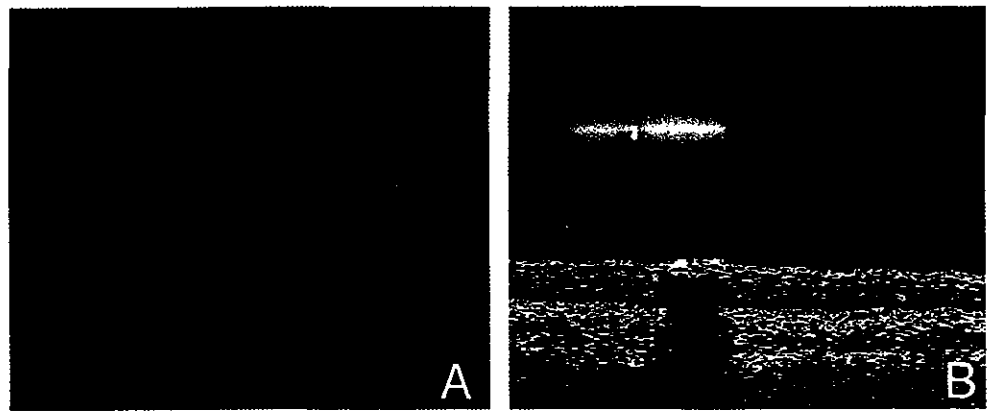

Fig. 3. Case 2. A, Fundus photograph of the right eye indicating a dark spot at the inferior paramacula. B, Optical coherence tomography (OCT) image in a horizontal section showing a highly reflected area in the superficial retina with lack of deeper reflectivity.

oval pigmented spot at the inferior paramacula (Figure 3). The OCT image showed a highly reflected area in the superficial retina and lack of deeper reflectivity. Humphrey visual field analyzer and SLO microperimetry could not detect any scotoma, indicating a superficial location of the pigmented lesion as seen in Case 1.

Discussion

The RPE hamartoma is a focal, nodular, jet-black lesion that usually involves the full thickness of the retina and spills onto the inner retinal surface in an umbrella fashion.[1] Intraretinal RPE hamartoma has been divided into three categories: superficial location, preretinal extension, and preretinal extension with superficial vascularization.[1] Among 10 eyes with unilateral RPE hamartomas described by Gass, the hamartoma was located juxtapapillary in one eye, eight eyes involved the paracentral macula, and one eye involved the central macula. Only the last case was symptomatic, being associated with poor vision (20/400) and esotropia.[1] In contrast, the current case with a central macular pigmentation (Case 1) showed no objectively detectable visual impairment. In our experience, an OCT image of CHRPE shows a highly reflected area beneath the sensory retina and lack of deeper reflectivity, which is apparently distinguishable with the images of RPE hamartomas in the current cases. In addition, we believe that the RPE hamartomas in our cases are restricted to location in the superficial retinal layer, leaving the other layers intact, unlike other types of RPE hamartoma.

Fluorescein angiography in Case 1 demonstrated a partial obstruction of the macular capillary network, which was different from the finding in a case of macular CHRPE, in which there was no obstruction of choroidal fluorescence.[5] The retinal fluorescein angiogram would be useful in differentiating these two diseases. However, if the whole lesion locates within a foveal avascular zone, hypofluorescence on the angiogram cannot predict a vertical location of the lesion. OCT may have an advantage in such a case, and microperimetry can detect the retinal function behind the high reflectivity shown in OCT. Although OCT does not describe fully the vertical extension of hamartomatous tissue as well as histologic analysis showing a high variability described by Gass,[1] noninvasive evaluations by a combination of OCT and SLO microperimetry are feasible to clearly illustrate the superficial location and the function of the lesion, respectively, in the RPE hamartomas of the current cases.

Key words: hamartoma, microperimetry, optical coherence tomography, pigmentation, retinal pigment epithelium.

Acknowledgments

The authors wish to thank Dr. Hans E. Grossniklaus for his assistance with diagnosis.

References

1. Gass JDM. Focal congenital anomalies of the retinal pigment epithelium. Eye 1989;3:1–18.
2. Yanoff M, Fine BS. Ocular Pathology, 5th ed. St. Louis, Mosby, 2002, pp 660–663.
3. Holz FG, Alexandridis E, Volcker HE, et al. Spontaneous incomplete avulsion of juxtafoveal retinal pigment epithelial hamartoma. Arch Ophthalmol 2001;119:903–907.
4. McDonald HR, Abrams GW, Bruke JM, et al. Clinicopathologic results of vitreous surgery for epiretinal membranes in patients with combined retinal and retinal pigment epithelial hamartomas. Am J Ophthalmol 1985;99:604–605.
5. Nishikatsu H, Shiono T. Congenital hypertrophy of the retinal pigment epithelium in the macula. Ophthalmologica 1996;210:126–128.

Evaluation of calcification of a hydrogel intraocular lens by optical coherence tomography

Shin Hatou, MD, Makoto Inoue, MD, Daijiro Kurosaka, MD, Yudi Richard Hida, MD, Kei Shinoda, MD, Yoshihisa Oguchi, MD

We describe 2 cases of calcification of hydrogel intraocular lenses (IOLs) evaluated by optical coherence tomography. Dense or slight surface opacities of hydrogel IOLs were detected initially by slitlamp biomicroscopy in a 55-year-old woman and a 77-year-old woman. The opacities resulted in complaints of hazy vision after uneventful phacoemulsification and IOL implantation. Optical coherence tomography was used to further assess the opacities and showed calcification by high reflectivity on the anterior and posterior IOL surfaces in the first patient and on the anterior surface in the second patient. No abnormal reflectivity was seen on the surface of a hydrophobic acrylic IOL in the second patient's fellow eye. Optical coherence tomography may be useful to detect calcification of a hydrogel IOL.

J Cataract Refract Surg 2004; 30:1590–1592 © 2004 ASCRS and ESCRS

Calcification of hydrogel or hydrophilic acrylic intraocular lenses (IOLs) is a recently identified postoperative complication that causes visual impairment after cataract surgery.[1–5] Histologically, the calcium appears as hydroxyapatite deposits on IOL surfaces.[1] We describe in vivo evaluation of calcified IOLs by optical coherence tomography (OCT).

Case Reports

Case 1

A 55-year-old Japanese woman was referred to us in 2003 for the diagnosis and treatment of visual impairment in the right eye. In 2001, the patient had successful vitreous surgery for proliferative diabetic retinopathy in the right eye. Six months later, she had uneventful cataract surgery that included phacoemulsification and implantation of a hydrogel IOL (Hydroview, Bausch & Lomb). The visual acuity was 20/250 after vitreous surgery and 20/50 after cataract surgery. In 2003, the visual acuity in the right eye was hand motions; the decrease in visual acuity may have been caused by optic atrophy from diabetic retinopathy. Slitlamp examination revealed a white opacity on the surface of the hydrogel IOL (Figure 1, *A*). Optical coherence tomography showed high reflectivity on the anterior and posterior surfaces of the IOL (Figure 2, *A*). The hydrogel IOL was replaced with a hydrophobic acrylic IOL, and the visual acuity recovered to 20/80.

Case 2

A 77-year-old Japanese woman with systemic hypertension complained of decreasing visual acuity in the left eye 3 years after uneventful cataract surgery. Ophthalmologic history in that eye was otherwise unremarkable. The visual acuity was 20/25 soon after cataract surgery but deteriorated to 20/200. Slitlamp examination revealed only faint reflectivity or haziness on the surface of the hydrogel IOL (Hydroview). The abnormality was too slight for a definitive diagnosis of calcification, although the generalized haziness on the IOL surface along with 2 forceps marks could have been the typical appearance of IOL calcification (Figure 1, *B*). The subtle opacity between the marks was far less dense than that in Case 1 (Figure 1, *B*). Optical coherence tomography showed high reflectivity on the anterior surface of the IOL but not on the posterior surface (Figure 2, *B*). Optical coherence tomography showed no remarkable findings on the

Accepted for publication November 25, 2003.

From the Department of Ophthalmology, Keio University School of Medicine, Tokyo, Japan.

None of the authors has a financial or proprietary interest in any material or method mentioned.

Reprint requests to Daijiro Kurosaka, MD, Department of Ophthalmology, Keio University School of Medicine, 35 Shinanomachi, Shinjyuku, Tokyo 160-8582, Japan. E-mail: kurosaka@sc.itc.keio.ac.jp.

0886-3350/04/$–see front matter
doi:10.1016/j.jcrs.2003.11.048

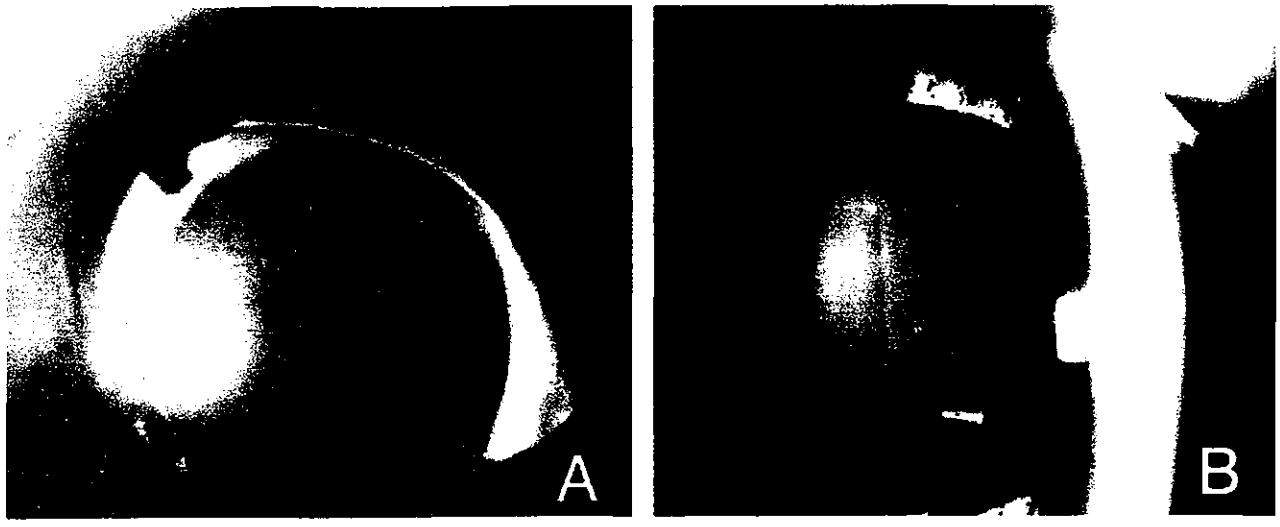

Figure 1. (Hatou) *A*: Slitlamp photograph of the right eye in Case 1. *B*: Slitlamp photograph of the left eye in Case 2. A white opacity is on the IOL surface in both cases, but Case 1 shows a greater density more readily interpreted as calcification than the findings, including 2 forceps marks, in Case 2.

IOL surface in the opposite right eye in which a hydrophobic acrylic IOL had been inserted but had not calcified. The calcified IOL in the left eye was replaced with a hydrophobic acrylic IOL, and the visual acuity recovered to 20/25.

Discussion

Calcification of hydrogel IOLs after implantation typically develops along the IOL surface at 12 to 25 months and often results in marked visual disturbance. Replacement of the calcified IOL is the only treatment that can restore visual acuity.[1–4] Intraocular lens calcification has been attributed to adhesion of silicone from the packing system to the IOL surface in combination with intraocular fatty acids.[5]

Fully developed calcification of an IOL can be evaluated by routine ophthalmic examinations including visual acuity testing, slitlamp examination, and fundoscopy. However, slight calcification may not be apparent or may be difficult to interpret with conventional examinations. Optical coherence tomography has been used extensively to obtain a precise longitudinal morphologic analysis of the anterior and posterior segments. This imaging modality clearly illustrated the subtle IOL calcification in Case 2, in contrast to the unremarkable OCT appearance of the contralateral acrylic IOL unaffected by calcification. We concluded that OCT detected increased reflectivity on the surface of the calcified IOLs. Since there may be other causes of reflectivity on IOL surfaces, further study is necessary to define the role of OCT in diagnosing this condition.

References

1. Fernando GT, Crayfold BB. Visually significant calcification of hydrogel intraocular lenses necessitating explantation. Clin Exp Ophthalmol 2000; 28:280–286

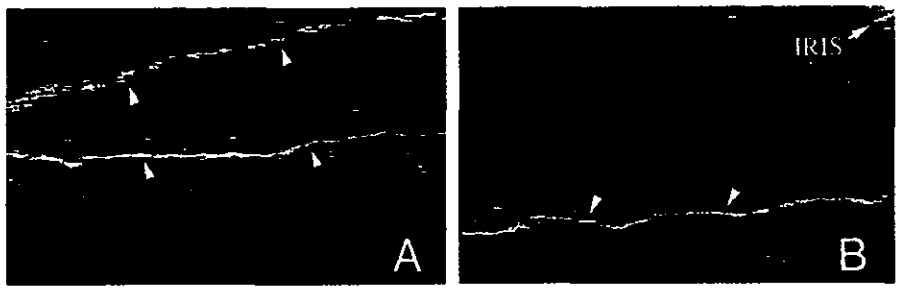

Figure 2. (Hatou) *A*: Optical coherence tomography of the right eye in Case 1. *B*: Optical coherence tomography of the left eye in Case 2. High reflectivity typical of calcification is seen on both IOL surfaces (anterior, arrowheads; posterior, arrows) in Case 1 but only on the anterior IOL surface in Case 2.